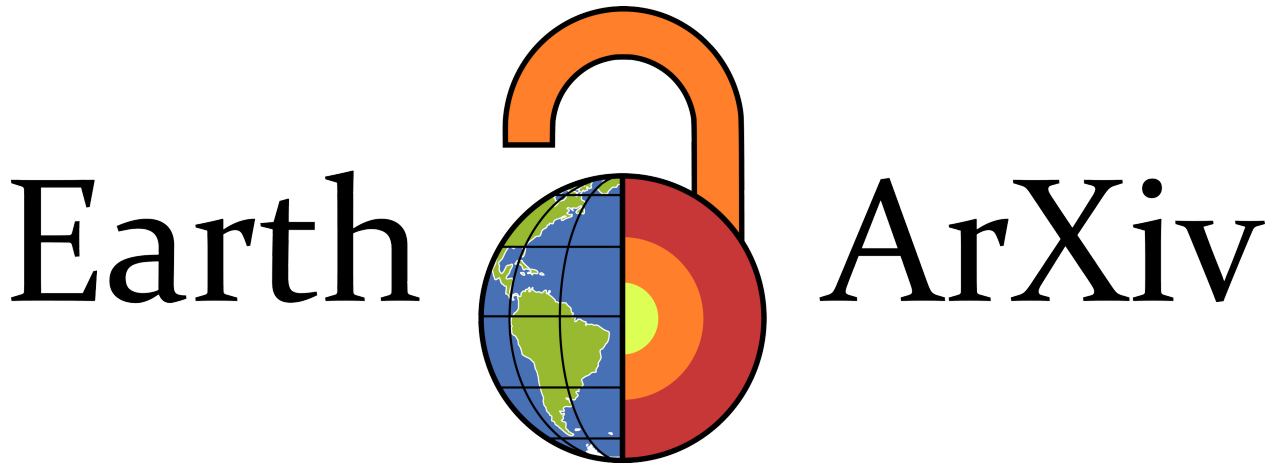

Thermodynamic modeling tools for the interpretation of melt inclusions and volcanic gases

Iacovino et al.

Thermodynamic modeling tools for the interpretation of melt inclusions and volcanic gases

Kayla Iacovino *[α], Ery Hughes[β,γ], Penny Wieser[δ], Alain Burgisser[ε], Philippa Liggins[ζ], Shuo Ding[η], Chenguang Sun[θ], and Geoff Kilgour[γ]

[α] Carl Sagan Center for Research, SETI Institute, Mountain View, CA, 94043, US.

[β] Department of Earth Sciences, University College London, London, WC1E 6BT, UK.

[γ] Earth Sciences New Zealand, Te Awa Kairangi ki Tai Lower Hutt, 3351, Aotearoa New Zealand.

[δ] Department of Earth and Planetary Science, University of California Berkeley, Berkeley, CA, US.

[ε] Univ. Grenoble Alpes, Univ. Savoie Mont Blanc, CNRS, IRD, Univ. Gustave Eiffel, ISTerre, Grenoble, 38000, France.

[ζ] University of Oxford, Oxford OX1 2JD, UK.

[η] University of Florida, Gainesville, FL, 32611, US.

[θ] University of Texas, Austin, TX, 78712, US.

Abstract

H_2O, CO_2, and S are the most abundant volatiles in basaltic magmatic systems and are critical to understanding magma storage and the size and style of volcanic eruptions. Models for calculating melt–vapor (±mineral) equilibria are abundant in the literature but are not interoperable. Consequently, few comparisons of model outputs have been performed. To address this, we comprehensively compare five H-O-C-S melt–vapor equilibrium tools (D-Compress, VolFe, EVo, Sulfur_X, MAGEC) to evaluate how and why they diverge. We present a series of degassing scenarios for MORB, Kīlauea, Fuego, and Fogo basalts revealing that often understated model assumptions such as fO_2 buffer equations and fO_2-$Fe^{3+}/\Sigma Fe$ relationships have outsized effects on results. All models consider both a reduced and oxidized sulfur melt species but with different approaches to incorporating their solubility. Differences in model implementation lead to clear output divergence of modeled gas compositions, melt S and Fe speciation, and fO_2. We also compare tool outputs with those of S-free models MagmaSat, VolatileCalc, and Iacono-Marziano using VESIcal and find that the addition of S has little to no effect on the calculation of the vapor saturation pressure (P^v_{sat}). Conversely, the calibration dataset underlying an H_2O–CO_2 model implemented into these tools exerts the strongest control on P^v_{sat} particularly for compositions less represented in the experimental literature (here, Fuego and Fogo). We recommend that new high temperature and pressure solubility experiments target the conditions where models most severely disagree rather than aiming to "fill in the gaps" in parameter space. The success of future assessments of model suitability rely on a continued push for regular evaluation of code usability, transparency, interoperability, and benchmarking. These factors must be the codified pillars of the peer-review process, providing the confidence for wider community uptake and implementation.

Keywords: Volcanic volatiles; Thermodynamic modeling; Melt inclusions; Volcanic degassing; Eruption monitoring; Magma evolution.

1 Introduction

Volcanic gases are the main drivers of volcanic eruptions and play a role in nearly every component of a magma's chemical evolution. In concert with seismic, deformation, and imagery data, volcano observatories rely on *in situ* and remote chemical

* kiacovino@seti.org

and flux measurements of volcanic gases to forecast whether a volcano will erupt and, if so, where, when, and how [Poland and Anderson 2020; Kern et al. 2022; Kilburn and Bell 2022; Acocella et al. 2024; Aiuppa et al. 2025a; Aiuppa et al. 2025b]. Broadly, because each volatile species has a distinct pressure-dependent solubility, changes in chemical ratios of gas emissions may signal deep magma recharge, which in turn may lead to an eruption [Giggenbach 1996; Aiuppa et al. 2007; De Moor et al. 2016]. Quantitatively interpreting gas measurements in the context of the state and activity of a particular volcanic system as a whole, however, requires a foundational understanding of the petrology of the magma at depth: its composition, volatile budget, pressure (P), temperature (T), and oxygen fugacity [fO_2, a measure of redox state; Aiuppa et al. 2007; Iacovino 2015; De Moor et al. 2016; Werner et al. 2020; Lerner et al. 2021b; Hughes et al. 2024a; Ding et al. 2025].

Two complementary data streams illuminate the volatile history of a magmatic system. At the surface, direct measurements of gas emission rates and compositions provide near-real-time information on degassing behavior [Fischer et al. 1996; Aiuppa et al. 2010b; Werner et al. 2011; Werner et al. 2013; Allard et al. 2016]. At depth, melt inclusions (MI) and fluid inclusions (FI) not only record the pressure at which crystallization and degassing processes occurred, but also preserve a snapshot of dissolved and exsolved volatile concentrations at the point of their entrapment [Roedder 1979; Lowenstern, Thompson, et al. 1995; Metrich and Wallace 2008; Rose-Koga et al. 2021; Wieser et al. 2021; 2025]. Together, these datasets represent geochemical bookends of an eruption from source to surface. Several studies have tested the power of combining MI and surface gas chemistry datasets by applying existing solubility models, sometimes in concert with new empirical or thermodynamic frameworks [Wardell et al. 2001; Shinohara et al. 2003; Burton et al. 2007; Aiuppa et al. 2010a; Oppenheimer et al. 2011; Iacovino 2015; Werner et al. 2020]. Aiuppa et al. [2007] used thermodynamic volatile solubility modeling [Moretti et al. 2003] to retrospectively interpret two years of continuous real-time volcanic gas measurements at Etna volcano. Their study unambiguously demonstrated that increasing CO_2/SO_2 gas ratios signaled the ascent of deep, CO_2-rich magmas, subsequently leading to over-pressurization and triggering of eruption.

The models underpinning these interpretations rest on decades of laboratory experiments that measure the equilibrium concentration of H-O-C-S species in a volatile-saturated silicate melt as a function of P, T, and melt composition. Early solubility models addressed H_2O and CO_2 either individually or in combination [e.g., Dixon 1997; Newman and Lowenstern 2002; Liu et al. 2005; Iacono-Marziano et al. 2012; Iacovino et al. 2013; Allison et al. 2019], and several tools now exist for mixed H_2O-CO_2 calculations [e.g., Newman and Lowenstern 2002; Ghiorso and Gualda 2015; Iacovino et al. 2021; Allison et al. 2022; Sun and Yao 2026]. Sulfur, despite being the volcanic gas most routinely measured at the surface, owing to its low atmospheric background and distinct UV signature [Oppenheimer 2010], has only recently been incorporated into multicomponent solubility models. Its omission is not surprising; sulfur can exist in valence states from S^{2-} to S^{6+}, each with its own solubility behavior that depends strongly on melt composition, and readily forms solid sulfide or sulfate phases in magmas, making both experiments and thermodynamic formulations considerably more complex [Fincham and Richardson 1954; Carroll and Rutherford 1985; O'Neill and Mavrogenes 2002; Jugo et al. 2005; Baker and Moretti 2011; Simon and Wilke 2026].

CHOSETTO [Moretti et al. 2003; Moretti and Papale 2004], the models of Gaillard et al. [2011] and Gaillard et al. [2013], SolEx [Witham et al. 2012], and D-Compress [Burgisser et al. 2015] are notable early tools for H_2O-CO_2-S solubility, although

SolEx uses a very simplified S model. Early modeling tools relied on the experimental literature and computational technology of the time, typically producing static non-extensible models that are difficult to unpack, reuse, and upgrade. D-Compress stands out as one of the earliest models to adopt a modern "extensible" ethos; it was built with the intention of allowing users to subsequently add new solubility laws. The decade since has seen a notable expansion of our experimental knowledge base, coinciding with the development of computational technologies that aid the construction of new open-source models, built using FAIR data principles [Wilkinson et al. 2016]. Now, a new generation of H-O-C-S volatile solubility models and tools has emerged, each implementing its own approach to S solubility, redox coupling, and melt-vapor partitioning [e.g., Liggins et al. 2020; 2022; Sun and Lee 2022; Ding et al. 2023; Ghiorso et al. 2023; Hughes et al. 2024b; Sun and Yao 2024; Hughes et al. 2025]. Additional tools are being purpose-built for extraterrestrial applications where conditions (particularly fO_2) differ from those common on Earth [Bower et al. 2025].

For users, traversing the range of melt–vapor equilibria tools is complex [Papale et al. 2022]. Many tools are tailored only to one volcano, to a narrow range of P–T–composition combinations, or simply handle each scenario differently (and, given the complexity of the models and the vast number of assumptions and choices that modelers need to make, this is often for mysterious, obfuscated reasons). As a result, running another group's model often requires familiarity with its internal conventions or direct correspondence with its authors, and unstated assumptions can quietly propagate into results. Tools that are the most user-friendly are thus heavily over-represented in the literature [e.g., VolatileCalc; Newman and Lowenstern 2002], even though they are often the least widely applicable, as demonstrated by Wieser et al. [2022].

Observatories like the Hawaiian Volcano Observatory have measured volcanic gases for over a century [Sutton and Elias 2014], and regular monitoring of gas chemistry is commonplace among major volcano observatories around the world. Despite access to these data, automated operational forecasting predominantly relies on seismic, deformation, and imagery observations, while gas data are often interpreted manually *a posteriori*. Gas chemistry is automatically ingested in some operational eruption forecasting tools used at observatories to support decision-making [e.g., in Aotearoa New Zealand for Ruapehu and Whakaari; Christophersen et al. 2022; Behr et al. 2025], but these systems are learned from monitoring data, eruption records, and expert elicitation rather than using derived outputs based on geochemical modeling. Mathematical models that could enable the use of gas measurements as interpretive tools for forecasting exist in principle but are, in practice, inaccessible to the people who need them most. This paper represents an effort to synthesize the range of models available so that errors are explored and recommendations for usage are clearly laid out. We systematically compare our modeling tools against one another in the context of MI and surface gas composition data, seeking to understand where and why models disagree, how sensitive their outputs are to seemingly innocuous assumptions, and what must be resolved before any of these tools can be responsibly deployed in an observatory setting.

Here we compare D-Compress [Burgisser et al. 2015], EVo [Liggins et al. 2020; 2022], MAGEC [Sun and Lee 2022; Sun and Yao 2024], Sulfur_X [Ding et al. 2023], and VolFe [Hughes et al. 2024b; Hughes et al. 2025] via a set of degassing scenarios for four basaltic magmatic systems: mid-ocean ridge basalt, ocean island basalts (Kīlauea and Fogo) and arc basalt (Fuego). We focus on basalts due to the abundance of experimental literature of mafic compositions relative to evolved and, even more so, to intermediate magmas. Where possible, H_2O-CO_2 models embedded in these tools are compared to the same

models implemented in VESIcal [Iacovino et al. 2021], which serves as a fully benchmarked reference but lacks any model for sulfur. We focus on the choices made in constructing each tool—databases, thermodynamic formulations, redox conversions, normalization routines, and computational methodologies—and the effects these choices have on outputs. We do not draw inferences as to which model produces the most "correct" results; rather, we use this exercise to lay the groundwork for a shared, modular, and transparent melt–vapor equilibria framework, and to argue that the evaluation of code usability, transparency, and benchmarking should be codified pillars of the peer-review process.

2 Modeling scenarios

2.1 Tools tested and choice of model options

Throughout the manuscript we use the term "tool" to refer to software or code that combines multiple models or equations. We reserve the term "model" to refer to an equation or set of equations that defines an equilibrium state of a system, defined either thermodynamically, empirically, or a combination of the two. This distinction is critical since each tool in reality contains an interconnected framework of model equations; the tool offers functionality via a documented, tested, and extensible code base and may itself implement additional empirical regression and/or thermodynamic relationships to facilitate the seamless combination of disparate models. A magma degassing modeling tool could, for example, contain an existing model for H_2O solubility coupled to a new model for CO_2 solubility. Open-source code allows for the interrogation of the choices made by the author of a tool, their implementations of models, and what data transformations are applied to input parameters.

Below we provide a brief introduction to all five S-degassing tools examined in this work. For the full details of each tool, we refer the reader to the original publications. Each tool includes various pre-existing H_2O-CO_2 models, which are coupled to sulfur models via custom tweaks or additions as necessary to meld the pre-existing model formulations with their own.

1. **D-Compress** [Burgisser et al. 2015] contains a thermodynamically based empirical model calibrated for calculating the melt–vapor equilibrium along a degassing path for basalts, phonolites, and rhyolites, with operational T ranging from 790 to 1400 °C. The code is written in Turbo Delphi 2006 with the BCD library Systools from TurboPower and was originally compiled for Windows OS (XP, Vista, 7). The software and user manuals are hosted on the Institut des Sciences de la Terre website*.

2. **EVo** v1.0.2 [Liggins et al. 2020; 2022] contains multiple thermodynamic models to simulate the degassing of H-O-C-S-N species, in both terrestrial and extra-terrestrial scenarios. The D-Compress model can be used within EVo, which is benchmarked against the original code. EVo is written in Python3 and has been tested on Windows, MacOS, and Linux. The source code and documentation are hosted on GitHub†.

3. **MAGEC** v1b [Sun and Lee 2022; Sun and Yao 2024] is a MATLAB-based melt-vapor equilibrium tool for C-H-O-S systems that solves coupled volatile mass balance, melt-vapor equilibria, and redox evolution during degassing and/or crystallization. The original framework [Sun and Lee 2022] incorporates chemical equilibria among vapor species, volatile dissolution in the melt, Fe- and S-redox reactions, non-ideal gas behavior, and optional constraints on graphite,

*https://www.isterre.fr/annuaire/pages-web-du-personnel/alain-burgisser/article/software.html
†https://github.com/pipliggins/EVo

sulfide, and sulfate saturation. The updated version [Sun and Yao 2024] implements Fe- and S-redox models calibrated over broad compositional ranges, including low- to high-SiO_2 melts, and allows users to specify initial redox using $\log f O_2$, $Fe^{3+}/\Sigma Fe$, $S^{6+}/\Sigma S$, ΔIW, ΔFMQ, or ΔNNO. MAGEC has also been evaluated against experimental solubility data and natural melt-inclusion and glass datasets, including MORB glasses [Sun and Lee 2022] and olivine-hosted melt inclusions from silica-undersaturated lavas [Sun and Yao 2024]. The setup file is a human-readable .m file, but the solver itself is compiled in MATLAB's .p file format and is not open source. It is available via the Texas Data Repository*.

4. **Sulfur_X** v1.2 [Ding et al. 2023] combines existing H-O-C degassing models with newly derived sulfur partition coefficients to simulate the degassing of H-O-C-S species in basalts and basaltic andesites. Two sulfur degassing reactions are used to develop predictive models of partition coefficients comprising a thermodynamically based empirical model, calibrated with experiments conducted at 1030–1300 °C and 1–5000 bars. The code is written in Python3. The source code and documentation is hosted on GitHub†.

5. **VolFe** v1.0.2 [Hughes et al. 2024b; Hughes et al. 2025] combines existing melt–vapor equilibrium models for both oxidized and reduced species in the system H-O-C-S and is applicable to both terrestrial and extra-terrestrial scenarios. The tool uses a thermodynamic framework to combine models for all species via a set of chemical reactions, each with an equilibrium constant that constrains the concentrations of reactants and products at equilibrium. The code is written in Python3. The source code and documentation is hosted on GitHub‡ and installable using PyPI.

All of the tools allow the user to select which model to use for either H_2O, CO_2, or combined H_2O–CO_2 solubility. The IM [Iacono-Marziano et al. 2012] model implementation was chosen for all tools that have this option for easier comparison in this study (D-Compress (IM), MAGEC, and Sulfur_X). It is notable that there are technically three versions of IM; the published paper provides two sets of coefficients (anhydrous and hydrous) depending on whether the mole fraction of H_2O is included in the NBO/O term. Additionally, the hydrous coefficients in the paper differ slightly from those in the supplied web application [see Iacovino et al. 2021; Wieser et al. 2022]. D-Compress (IM), Sulfur_X, and VESIcal (IM) use the hydrous parameters in Table 6 of Iacono-Marziano et al. [2012], while MAGEC uses the hydrous web-app parameters. VESIcal additionally has options to use any existing IM parameters. VolFe calculations used their own in-house H_2O and CO_2 models [Hughes et al. 2024b], and the thermodynamic parameters for the closest melt composition of interest were chosen for CO_2: MORB, Kīlauea, and Fuego use parameters from Dixon et al. [1995] and Fogo uses Thibault and Holloway [1994]. EVo calculations used the D-Compress model for H_2O and CO_2, which we compare to additional D-Compress model runs using its in-house models [Burgisser et al. 2015].

Some calculations are additionally compared against the H_2O–CO_2 models of VolatileCalc [Newman and Lowenstern 2002, "VolatileCalc" or "VC"], Iacono-Marziano et al. [2012, "IM"], and MagmaSat [Ghiorso and Gualda 2015, "MagmaSat"] within VESIcal v1.2.11 [Iacovino et al. 2021], a thermodynamic model engine that also includes the models of Moore et al. [1998], Liu et al. [2005], Shishkina et al. [2014], and Allison et al. [2019]. In VESIcal, any one of seven models can be chosen to

*https://doi.org/10.18738/T8/LIKH3A
†https://github.com/sdecho/Sulfur_X
‡https://github.com/eryhughes/VolFe

model H_2O and/or CO_2 solubility, and all models are interchangeable. However, VESIcal does not contain models for sulfur solubility and most models do not consider redox [although MagmaSat accepts melt Fe^{3+}/Fe_T as an input; Wieser et al. 2022]. Each model implemented in VESIcal has been fully bench-marked against modeling results within the original publication of the model code or equation. The comparison of results from our degassing simulations to the H_2O–CO_2 results from VESIcal thus provide an S-free baseline for comparison to the tools implementing these models.

The Supplementary Material provides a list of the model options employed in our degassing scenarios. Most tools include other model options not tested here. As these tools are developed, the available model options evolve, so please refer to the tools themselves for the most up to date list. Throughout the manuscript we refer to all models with their given name and/or citation in the first instance, and then only as its given name (e.g., "VolatileCalc") or as the last name of the first author of the manuscript that first described it (see Supplementary Material for a full list).

2.2 Modeling approaches

All tools are based on the 'equilibrium and mass balance method' [Holloway 1987], but the approaches to modeling sulfur solubility with respect to a vapor phase are highly varied across the tools. Sulfur transitions from S^{2-}- to S^{6+}-dominant over the relatively narrow range of fO_2 encompassing most natural terrestrial systems, centered approximately near the Fayalite-Magnetite-Quartz (FMQ) buffer [Carroll and Rutherford 1988; Wallace and Carmichael 1994; Jugo et al. 2005]. This requires that dissolved S^{2-} and S^{6+} end-members be considered in the melt and both H_2S and SO_2 (at a minimum) be considered in the vapor. Tools differ in their implementations of sulfur species in the melt and vapor, reactions between melt and vapor, and formulations of the parameterizations considered. D-Compress assumes the concentrations (w) of H_2S and SO_2 in the melt are proportional to their fugacity (f) in the vapor by a power law:

$$w_i^m = a_i f_i^{b_i} \tag{1}$$

where i is H_2S or SO_2 and a and b are empirical constants as described in Table 1 of Burgisser et al. [2015]. In our degassing scenarios, S_2 is considered insoluble.

For reduced dissolved sulfur (sulfide, S^{2-}), MAGEC, EVo, and VolFe use the "capacity" approach ($C_{S^{2-}}$), which gives the maximum concentration of dissolved sulfide that can exist in a silicate melt at a given P, T, fO_2, and fS_2, based on the reaction of sulfide displacing oxide in the melt [Fincham and Richardson 1954]:

$$0.5S_2(v) + O^{2-}(m) = 0.5O_2(v) + S^{2-}(m) \tag{2}$$

$$w_{S^{2-}}^m = C_{S^{2-}} f_{O_2}^{-0.5} f_{S_2}^{0.5} \tag{3}$$

Note that a similar reaction can be written with SO_2 instead of S_2 as these vapor species are related through the following homogeneous vapor reaction:

$$0.5S_2(v) + O_2(v) = SO_2(v) \tag{4}$$

governed by an equilibrium constant (K):

$$K_{SO_2(v)} = \frac{fSO_2}{fS_2^{0.5} fO_2} \tag{5}$$

MAGEC, EVo, and VolFe implement various sulfide capacity models from the literature, which are empirically derived from experiments at controlled fO_2 and fS_2 [e.g., Nzotta et al. 1999; O'Neill and Mavrogenes 2002; O'Neill 2021; Boulliung and Wood 2023; Gorojovsky and Wood 2026; Thomas and Wood 2026].

Oxidized sulfur (sulfate, S^{6+} or SO_4^{2-}) is assumed to dissolve according to:

$$0.5S_2(v) + 1.5O_2(v) + O^{2-}(m) = SO_4^{2-}(m) \tag{6}$$

These three tools use different approaches to incorporate this. VolFe uses sulfate capacities ($C_{S^{6+}}$) from the literature [e.g., Boulliung and Wood 2022; O'Neill and Mavrogenes 2022; Boulliung and Wood 2023; Gorojovsky and Wood 2026; Thomas and Wood 2026], analogous to the sulfide capacity:

$$w^m_{S^{6+}} = C_{S^{6+}} f_{O_2}^{1.5} f_{S_2}^{0.5} \tag{7}$$

VolFe additionally considers an H_2S melt species using a similar approach to D-Compress (i.e., calculated as in eq. 1 but b_{H_2S} must equal 1) using in-house models [Hughes et al. 2024b].

MAGEC includes its own S-redox model [Sun and Yao 2024], which relates S^{6+}/S^{2-} to redox state, temperature, and melt composition, while also allowing users to choose among previous S-redox parameterizations. EVo uses S redox models from the literature [e.g., Jugo et al. 2010; Nash et al. 2019; O'Neill and Mavrogenes 2022; Boulliung and Wood 2023] that relate S^{6+}/S^{2-} to Fe^{3+}/Fe^{2+}:

$$\log_{10}\left(\frac{S^{6+}}{S^{2-}}\right)_m = 2\log_{10}(fO_2) + A = 8\log_{10}\left(\frac{Fe^{3+}}{Fe^{2+}}\right)_m + B \tag{8}$$

where A and B depend on melt composition, T, and P.

Sulfur_X calculates how the system's sulfur budget partitions between melt and vapor phases, irrespective of the total mass of sulfur, using a partition coefficient (K_D). The value of K_D is highly variable across P, T, melt composition, and fO_2 space [e.g., Webster and Botcharnikov 2011]. Sulfur_X implements a set of thermodynamic equations parameterized by empirically derived partition coefficients resulting in equilibrium equations for reduced (red) and oxidized (ox) S species of the form:

$$FeS(m) + H_2O(v) = H_2S(v) + FeO(m) \tag{9}$$

$$kdS^{v/m}_{red} = \frac{X_{H_2S(v)}}{X_{S^{2-}(m)}} \tag{10}$$

$$CaSO_4(m) = SO_2(v) + O_2(v) + CaO(m) \quad (11)$$

$$K_D S_{ox}^{v/m} = \frac{X_{SO_2(v)}}{X_{S^{6+}(m)}} \quad (12)$$

as outlined in Table 3 of Ding et al. [2023], where X is the mole fraction. Note that eq. 11 is equivalent to eq. 6 just specified for Ca and eq. 9 is related to eq. 2 through homogeneous vapor equilibria, e.g.:

$$0.5S_2(v) + H_2O(v) = H_2S(v) + 0.5O_2(v) \quad (13)$$

This results in an effective "combined" K_D, thermodynamically dictated by weighting the K_D's from either equilibrium reaction proportionally to the melt's $S^{6+}/\Sigma S$:

$$K_D S_{combined}^{v/m} = \left(1 - \frac{S^{6+}}{\Sigma S}\right) K_D S_{red}^{v/m} + \left(\frac{S^{6+}}{\Sigma S}\right) K_D S_{ox}^{v/m} \quad (14)$$

The melt $S^{6+}/\Sigma S$ is calculated from S-Fe redox models from the literature [e.g., Nash et al. 2019; Muth and Wallace 2021; O'Neill and Mavrogenes 2022]. Details of all settings for all model runs are in the Supplementary Material.

2.3 Choice of computations and initial conditions

All of the tools examined can perform a number of thermodynamic calculations with regards to the equilibrium state of a defined melt–vapor system. We chose to calculate a closed-system, isothermal, decompression-induced magma degassing path from the tool-calculated pressure of vapor saturation (P_{sat}^{v}) for each starting composition described in Section 2.4. This type of calculation incorporates:

1. the calculation of P_{sat}^{v};
2. the speciation of S at various melt redox states;
3. the calculation of the equilibrium melt–vapor composition and the proportions of melt and vapor in the system; and
4. equilibrium calculations in a series of steps as P decreases from the point of vapor saturation to 1 bar.

The latter allows us to see how each tool handles system evolution and whether errors or divergence of results are compounded as each model scenario progresses down-P. The use of multiple basaltic systems allows us to interrogate the compositional dependence of each model as implemented in each tool. A representative temperature was selected for each system, and held constant during the model run, simulating isothermal decompression.

We chose to begin our degassing paths at the P_{sat}^{v} as calculated by the tool, rather than prescribing a particular starting P. This reflects how degassing models are commonly used by the community: the initial P is not known *a priori*, but volatile concentrations can be measured in physical samples like melt inclusions. For all tools except D-Compress, the starting P is the first value calculated. D-Compress uses the alternative method of asking the user to specify the total P and outputs the

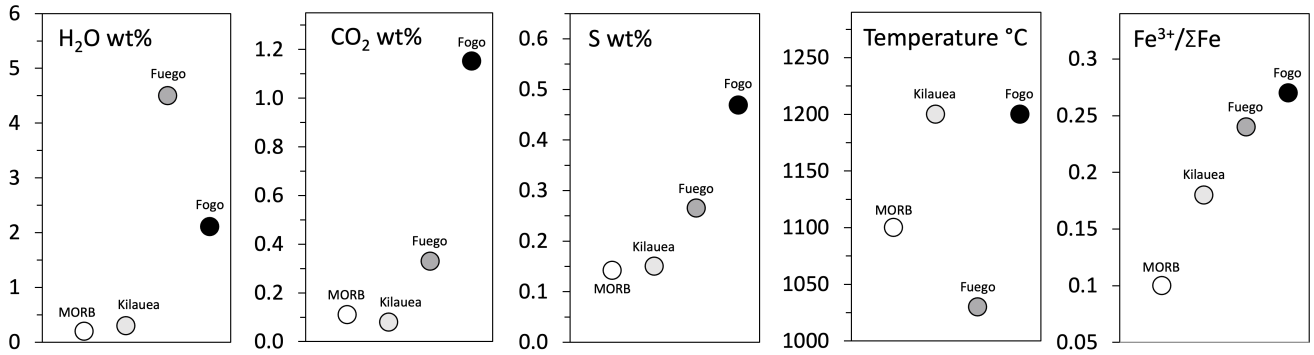

Figure 1: Matrix of starting parameters chosen for each basaltic system for all degassing simulations. Numerical values provided to all tool authors are given in Table 1. The redox value for Fogo was given to the authors as ΔNNO+0.7 and converted to $Fe^{3+}/\Sigma Fe$ using the Kress and Carmichael [1991] calculator of Iacovino [2021] at 5000 bar in this figure.

amount of dissolved S that would cause vapor saturation. This method requires the user to manually adjust *P* until the desired value of S is obtained. This adjustment is tedious because often the correct *P* is reached in an asymptotic manner, yielding initial *P* values with many significant digits.

In the literature, redox of a natural system is commonly reported in one of several possible formats, and tools can accept only some of those (see Supplement). This means that the translation of the reported value to one allowed by any tool is often required of the user before modeling can begin. This is also true of our benchmark simulations. For most of our calculations, $Fe^{3+}/\Sigma Fe$ is the given redox variable, as might be measured in MI. For Fogo, the only reported constraints on melt redox are expressed relative to the Nickel-Nickel Oxide (NNO) buffer [DeVitre et al. 2023], as is true for many volcanoes around the world given logistical challenges in directly measuring Fe and S redox in melts. This presents an excellent opportunity to compare the way different tools handle the relationship between buffer value and Fe or S speciation and, indeed, how they might translate between two buffer values. Our choice to use the NNO buffer as our initial condition for Fogo introduces an additional *a priori* uncertainty to degassing simulations that take ΔFMQ as a model input since the conversion between two buffers is *P*-dependent; a critical consideration since *P* is not an input but rather the first calculated output in most simulations. As *P* is determined from measured volatile content, not all models have matching initial redox conditions.

2.3.1 *Options not explored*

EVo, MAGEC, Sulfur_X, and VolFe have options to model sulfide, anhydrite, and graphite saturation. In our model runs, these saturation limits were turned off such that no solid phases precipitate, allowing for more direct comparisons of degassing behavior. Incorporating sulfide and sulfate saturation would introduce significant complexity, given the wide range of models that can be used to calculate these saturation limits, and their sensitivity to melt composition, sulfide composition, *T*, and *P* [Wieser et al. 2020]. The amount of sulfide and sulfate precipitation is also extremely sensitive to the speciation of S. Sulfur_X and MAGEC can also incorporate the effects of silicate crystallization, which we also turn off in these calculations.

2.4 Choice of volcanic systems

Four basaltic volcanic systems were chosen to represent a range of tectonic settings, bulk and volatile element contents, *T*, and redox conditions: mid-ocean ridge basalt (MORB), volatile-poor ocean island basalt (OIB, Kīlauea), volatile-rich OIB (Fogo),

Table 1: Initial conditions used as inputs for all model runs. For redox values, if any tool required an input in a different form to what we specify, the tool's author first translated the specified value into something ingestible by their tool.

	unit	MORB	Kīlauea	Fuego	Fogo
Setting		MOR	OIB	Arc	OIB
SiO_2	wt%	47.40	50.19	51.46	42.40
TiO_2	wt%	1.01	2.34	1.06	3.26
Al_2O_3	wt%	17.64	12.79	17.43	11.17
FeO_T	wt%	7.98	11.34	9.42	12.00
MnO	wt%	0.00	0.18	0.19	0.14
MgO	wt%	7.63	9.23	3.78	9.55
CaO	wt%	12.44	10.44	7.99	13.31
Na_2O	wt%	2.65	2.39	3.47	3.36
K_2O	wt%	0.03	0.43	0.78	1.57
P_2O_5	wt%	0.08	0.27	0.24	0.75
Total	wt%	96.86	99.62	95.82	97.51
H_2O	wt%	0.20	0.30	4.5	2.11
CO_2	ppm	1100	800	3300	11520
S	ppm	1420	1500	2650	4690
Redox	$Fe^{3+}/\Sigma Fe$ or ΔNNO	0.10	0.18	0.24	NNO+0.7
T	°C	1100	1200	1030	1200

References: MORB majors: Allan et al. 1989; Ghiorso and Gualda 2015; Wieser et al. 2022. MORB volatiles, redox, and temperature: Cottrell et al. 2021. Kīlauea majors, volatiles, and T: Wieser et al. 2021. Kīlauea redox: Lerner et al. 2021b. Fuego majors: Lloyd et al. 2013; Moore et al. 2015; Newcombe et al. 2020; Rasmussen et al. 2020. Fuego volatiles: Rasmussen et al. 2020. Fuego redox and T: Lloyd et al. 2013. Fogo: DeVitre et al. 2023.

and arc basalt (Fuego). An overview of variables used for modeling is given in Table 1 and plotted in Figure 1. Here we only consider basaltic systems due to a significantly higher abundance of experimental and model data on these systems compared to more evolved melts. In mafic MI, a large proportion of the total CO_2 content of MI is held in vapor bubbles formed after MI entrapment. Because of the extreme sensitivity of CO_2 solubility to P, accounting for total CO_2 in the system, representative of entrapment conditions, is vital to correctly determine degassing trajectories [e.g., Moore et al. 2015; Rasmussen et al. 2020; Wieser et al. 2021]. We have focused on volcanic systems where CO_2 contents were measured both in the glass and co-existing bubble by Raman spectroscopy or experimental homogenization. All data used to arrive at our starting compositions, including individual melt inclusion measurements used to determine a composition representative of that eruption, are provided in the supplementary material.

Mid-ocean ridge basalts are represented by whole rock lava samples and representative MORB volatile concentrations. Major element data are from Lamont Seamount Chain lavas and adjacent East Pacific Rise lavas originally reported in Allan et al. [1989]. This is the same composition used in the parametrization database for MagmaSat MELTS [Ghiorso and Gualda 2015] and in the review by Wieser et al. [2022]. Temperature and volatile contents were chosen from representative MORB samples reported in Cottrell et al. [2021]. $Fe^{3+}/\Sigma Fe$ was set at 0.1, reflective of the majority of mid-ocean ridge basalts recording fO_2 around FMQ [Cottrell et al. 2021]. MORB lavas represent a volatile-poor end-member and position MORB as the most relevant to magma ocean and extraterrestrial model scenarios compared to other basalts examined here.

Major and volatile element compositions for all other samples are from glassy MI and include CO_2 abundances in vapor bubbles within MI. CO_2 we report here and use in modeling is the sum of the dissolved CO_2 in the melt and the exsolved CO_2 in the vapor bubble. Because they record the state of the melt at various points during crystal growth, MI are commonly paired with volatile solubility models to assess magma evolution and degassing patterns, including estimations of pre-eruptive magma conditions. As such, MI provide evidence-based starting conditions for magmatic degassing scenarios.

Volatile-poor OIBs are represented by Kīlauea volcano, Hawai'i. The volatile and redox systematics of Kīlauea magmas have been extensively studied using both olivine-hosted MI [Sides et al. 2014; Moore et al. 2015; Moussallam et al. 2016; Tucker et al. 2019; Lerner et al. 2021a; b; Wieser et al. 2021] and submarine glasses [Dixon et al. 1991; Clague et al. 1995], making them an ideal target for model inter-comparison. It is noteworthy that Kīlauean melts show variable H_2O contents, with some eruptions mostly yielding 0.3 wt%, and others 0.5–1.0 wt%. To address these variable H_2O contents, we performed two different Kīlauea models, Kīlauea 'dry' with 0.3 wt%, and 'wet' with 0.6 wt%. No significant differences were observed between these two runs, and so only the 'dry' runs are presented here. The major elements were chosen to be representative of higher MgO (10.2 wt%) MI corrected for post-entrapment crystallization [Wieser et al. 2020; Lerner et al. 2021a; Wieser et al. 2021]. The chosen initial CO_2 concentration of 800 ppm represents the most CO_2-rich MI from the 2018 eruption. For S, we use a concentration of 1500 ppm after Wieser et al. [2020] and Sides et al. [2014]. $Fe^{3+}/\Sigma Fe$ was set at 0.18 following Lerner et al. [2021b] and T at 1200 °C using the Helz and Thornber [1987] thermometer.

Oxidized H_2O-rich arc basalts are represented by Fuego volcano, Guatemala. Fuego MI from the 1974 eruption have up to 4.5 wt% H_2O [Rasmussen et al. 2020], relatively elevated S contents (2650 ppm) with up to 0.7 $S^{6+}/\Sigma S$ [Taracsák et al. 2023], and experimentally reconstructed CO_2 concentrations up to 3500 ppm [Rasmussen et al. 2020]. The major element composition representing Fuego is based on a compilation of data from Rasmussen et al. [2020], Lloyd et al. [2013], Moore et al. [2015], and Newcombe et al. [2020], whilst volatiles are from Rasmussen et al. [2020]. $Fe^{3+}/\Sigma Fe$ was set at 0.24 and T at 1030 °C following Lloyd et al. [2013] and Ding et al. [2023].

Volatile-rich OIBs are represented by Fogo Volcano, Cabo Verde, an end-member volcano representing one of the world's most volatile- and alkali-rich silica-undersaturated ocean island volcanoes. Fogo magmas have extremely high CO_2 and S contents (1.15 wt% and 4690 ppm, respectively) relative to other OIBs [DeVitre et al. 2023]. The major element composition was chosen as the average composition of 5 PEC-corrected melt inclusions from sample FG18 with the highest H_2O and CO_2 contents [DeVitre et al. 2023]. We take the redox conditions to be ΔNNO+0.7, as calculated by DeVitre et al. [2023] using the V partitioning oximeter of Canil [2002]. All values—majors, volatiles, redox, and T—are taken from DeVitre et al. [2023].

3 Modeling results

Model results from all tools for each basaltic system are compared based on the evolution of multiple P-dependent variables during magma degassing. These comparisons are not designed to assess model accuracy, but to quantify the degree of agreement between tools.

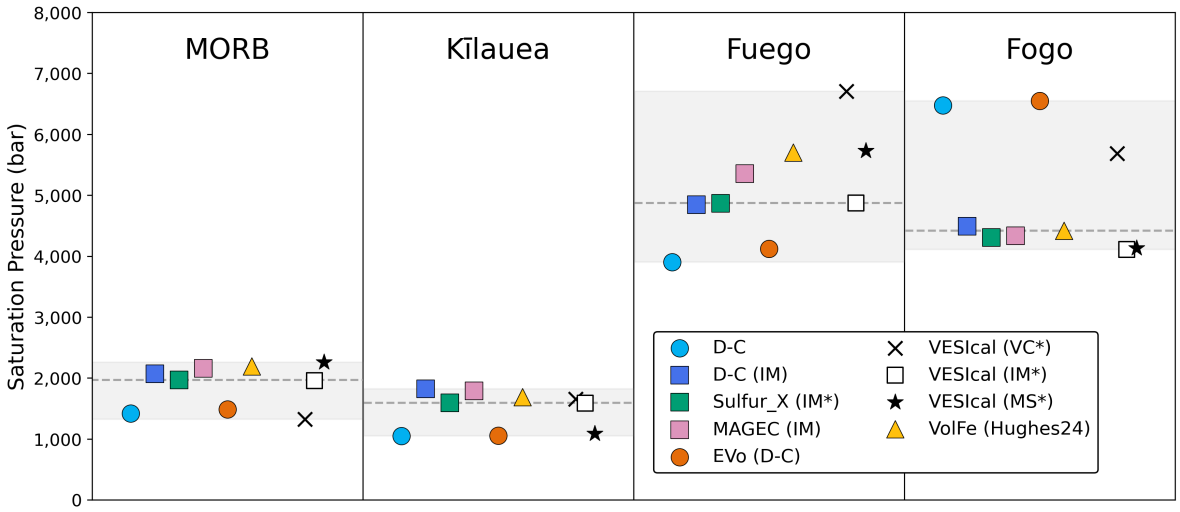

Figure 2: Pressure of vapor saturation (P^v_{sat}) calculated with each tool for all four basaltic systems. Also plotted are P^v_{sat} calculated by the VolatileCalc, Iacono-Marziano, and MagmaSat models using VESIcal. A separate color is used for each model, and these colors are consistent throughout the manuscript. Gray dashed lines represent the median, and the gray region shows the total range of values. Symbol shape corresponds to the underlying H_2O–CO_2 model used for degassing simulations in this work and is indicated in the legend. A * symbol indicates that pressure was calculated using H_2O and CO_2 concentrations only (no sulfur). The x-axes have no numerical significance and are only used to avoid symbol overlap.

Table 2: Vapor saturation pressure (P^v_{sat}, in bars) and equivalent depth (km) calculated by each tool for each basalt. Depths are relative to the volcanic vent (or sea level for MORB) and are derived from each tool's saturation pressure using the crustal density profiles described in the text.

Tool	MORB		Kīlauea		Fuego		Fogo	
	bars	km	bars	km	bars	km	bars	km
D-Compress	1420	6.8	1051	4.7	3900	15.1	6473	22.8
D-Compress (IM)	2068	9.1	1820	8.1	4844	18.5	4490	16.3
EVo	1484	7.0	1055	4.7	4121	15.9	6546	23.1
MAGEC	2157	9.4	1789	7.9	5353	20.4	4331	15.8
Sulfur_X	1968	8.7	1593	7.1	4863	18.6	4307	15.7
VolFe	2194	9.5	1689	7.5	5702	21.7	4417	16.1
VESIcal (IM)	1959	8.7	1587	7.0	4871	18.6	4111	15.1
VESIcal (VC)	1324	6.5	1654	7.3	6706	25.3	5687	20.3
VESIcal (MS)	2260	9.7	1090	4.8	5730	21.8	4130	15.1
Minimum	1324	6.5	1051	4.7	3900	15.1	4111	15.1
Median	1968	8.7	1593	7.1	4871	18.6	4417	16.1
Maximum	2260	9.7	1820	8.1	6706	25.3	6546	23.1

3.1 Pressure of vapor saturation

We can first examine the initial state of the system as determined by each tool by comparing the calculated P^v_{sat} (Figure 2 and Table 2). All tools calculate P^v_{sat} using mixed H_2O–CO_2-S solubility, except Sulfur_X, which uses the Iacono-Marziano H_2O–CO_2 model and VESIcal sub-models, which are S-free. We can directly compare S-free pressures from Sulfur_X and VESIcal (IM) to S-bearing pressures from D-Compress (IM) and MAGEC, which both utilize Iacono-Marziano for H and C in addition to solubility terms for S. All four models show consistent, strong agreement, indicating that sulfur has no discernible effect on calculated saturation pressure, consistent with the findings of Hughes et al. [2024b, although at low H_2O–CO_2 concentrations and when both S^{2-} and S^{6+} melt species are present, the effect of S on P^v_{sat} can become important].

Across all systems, P^v_{sat} estimates span 1324–6706 bars depending on the tool used (MORB: 1324–2260 bars; Kīlauea: 1051–1820 bars; Fuego: 3900–6706 bars; Fogo: 4111–6546 bars). Equivalent depths of degassing are calculated from saturation pressures using a two-layer hydrostatic model for each system, with densities and layer thicknesses informed by geophysical observations (Table 2). For MORB, we assume 2.75 km of seawater (1 g/cm^3) overlying basaltic crust (2.9 g/cm^3) after Theunissen et al. [2022]. For Kīlauea, a uniform density of 2.3 g/cm^3 is applied following the bulk above-sea-level edifice density of Denlinger and Flinders [2022]. For Fuego, we adopt a shallow crustal density of 2.38 g/cm^3 transitioning to 2.8 g/cm^3 at 6 km depth after Mickus [2003]. For Fogo, we use 2.7 g/cm^3 throughout the basaltic crust transitioning to 3.1 g/cm^3 at the moho at a depth of 12 km after Forte et al. [2023]. This translates to depth estimates relative to the volcanic vent (or sea level for MORB) ranging from 6.5–9.7 km for MORB, 4.7–8.1 km for Kīlauea, 15.1–25.3 km for Fuego, and 15.1–23.1 km for Fogo using the selected initial volatile contents (typically the highest representative concentrations in the melt inclusion datasets used to set degassing initial conditions). This means that the inferred magma chamber depth for each basaltic system can vary by a factor of ~1.7 depending on the solubility model chosen. This holds regardless of whether sulfur is considered in that calculation.

For Fogo, P^v_{sat} values calculated by EVo, D-Compress, and to a lesser extent VESIcal (VC), are significantly higher than those of all other tools, whose values cluster tightly around 4300 bars. It is tempting to treat EVo and D-Compress as outliers for Fogo. Their values are >2σ above the mean, and, if they were excluded, the other tools would show excellent agreement with values within <8% relative to the mean. This finding is particularly elucidating given Fogo's relatively "unusual" composition: a basanite with 42.4 wt% SiO_2 and 4.93 wt% Na_2O+K_2O [Le Maitre et al. 2005] and its extremely high CO_2 and S concentrations. This is a salient example justifying our choice to avoid declaring any model as being more "correct" than any other. Labeling EVo, D-Compress, and VESIcal (VC) as outliers implies that they are less reliable, when in fact, the opposite may be true. Modeling tools contain compositionally complex underlying experimental datasets and implement model equations that themselves sit atop even more data. Disentangling the appropriate compositional range over which tools are applicable thus becomes non-trivial. Nonetheless, we can consider broad differences in underlying datasets parameterizing each tool. The EVo runs conducted here use the H_2O and CO_2 solubility laws published by Burgisser et al. [2015] for D-Compress. In the underlying dataset, experiments on alkali-rich and silica-poor magmas are well-represented, ranging from 1.80–3.42 wt% Na_2O, 1.90–5.55 wt% K_2O, and 47.95–49.82 wt% SiO_2 [Beermann et al. 2011; Botcharnikov et al. 2011; Lesne et al. 2011a; b]. VolatileCalc is parameterized exclusively on alkali basalts and basanites [Dixon 1997; Newman and Lowenstern

2002]. The database of Iacono-Marziano [Iacono-Marziano et al. 2012] does have some alkali basalts, but it contains no basalts with SiO_2 <45 wt%, and most of the dataset basalts have Na_2O+K_2O <6 wt%. We can also consider the model of Allison et al. [2019], who performed H_2O–CO_2 experiments on several alkali-rich basalts. While none of the basalts have SiO_2 <47 wt%, all have Na_2O+K_2O >4 wt%. The Allison model as implemented in VESIcal ["AllisonCarbon"; Allison et al. 2019] predicts a saturation pressure of 7564 bars for Fogo, even higher than EVo. A thorough investigation of the effect of silica and alkali content on the results of all tools may shed light on which tool better predicts known pressures from H_2O–CO_2 solubility experiments performed on basanites like Fogo. This also serves as an example of how interoperable modeling tools would enable informed assessment of which gaps in our experimental databases are the most critical to fill.

3.2 Volatile concentrations in the melt: H_2O, CO_2, and S_T

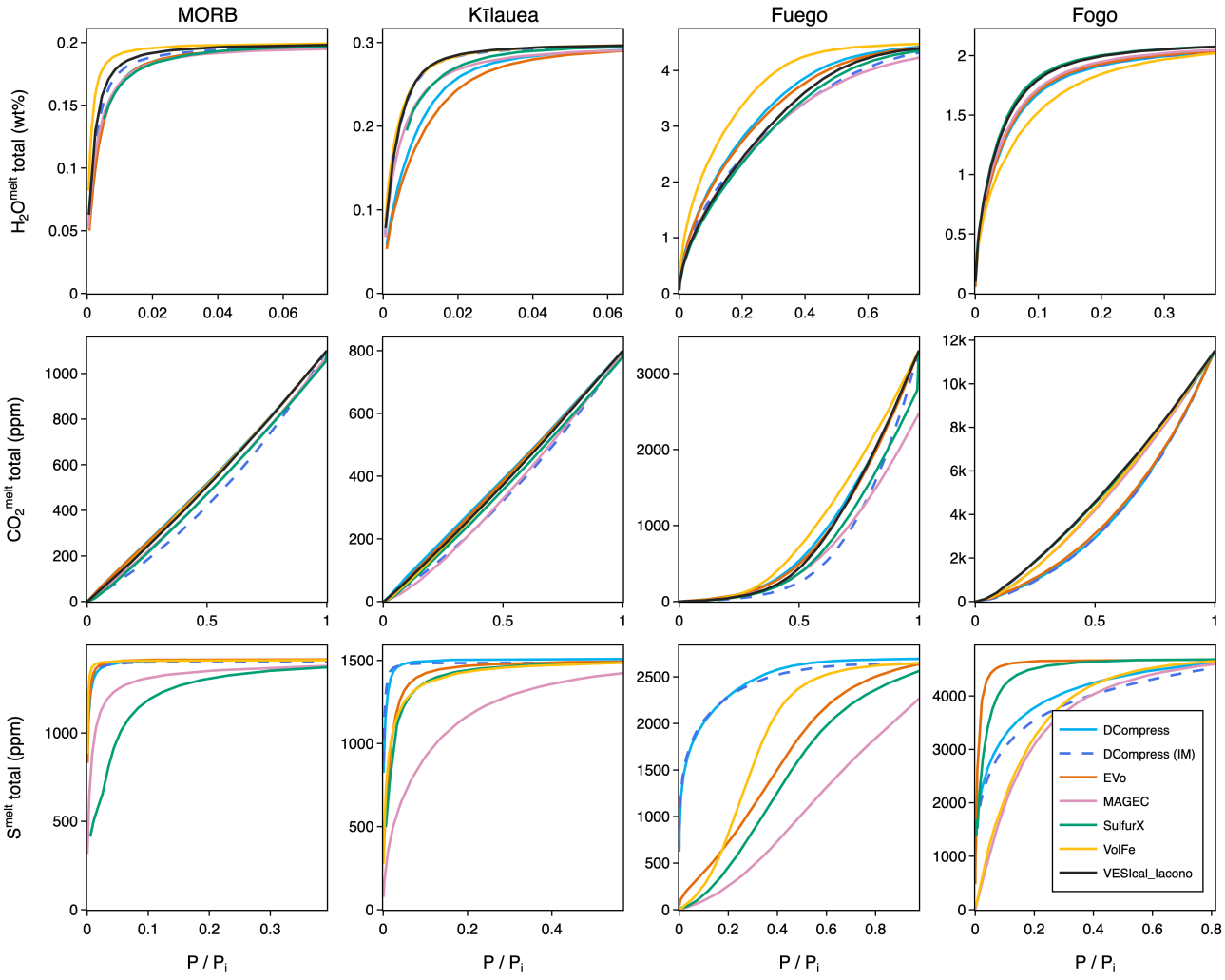

Figure 3: H_2O total, CO_2 total, and S total concentrations in the melt as a function of normalized pressure during degassing runs with all tools. Modeled dissolved melt H_2O and CO_2 are also shown for runs using the VESIcal implementation of the Iacono-Marziano model, which only considers H and C (black line). Note that x-axis maximum values are cropped to the point of the onset of significant degassing and differ between plots.

Because all degassing simulations begin degassing at the P of P^v_{sat}, the choice of underlying H_2O–CO_2 model and implementation thereof is at times the most important consideration for modelers, for example when comparing melt inclusion

data with other geochemical or geophysical observations of the magmatic system. The differences in calculated P^v_{sat} values between models thus obscure how modeled degassing paths evolve down-P. In the following analyses of degassing paths, we compare models in terms of normalized P calculated at each degassing step as P/P_i, where P is the pressure at the current step and P_i is the starting pressure, here P^v_{sat}.

Degassing curves showing the change in H_2O, CO_2, and S in the melt as a function of normalized P are shown in Figure 3. Volatiles are plotted in terms of the total budget of all species of each H, C, and S cast as H_2O, CO_2, and S. That is, the value for H_2O includes H from H_2O, OH^-, and H_2; and CO_2 may include CO if present.

For all species, results follow a common trend: tools agree strongly for MORB and Kīlauea, moderately well for Fogo, and very poorly for Fuego. For H_2O, CO_2, and S, both MORB and Kīlauea exemplify the canonical behavior of H_2O and S remaining dissolved in the melt until very shallow depths; and CO_2 is degassing throughout and linearly with decreasing pressure due to its lower solubility. For Fuego and Fogo, H_2O and CO_2 degassing show significantly more tool disagreement, significantly deeper degassing of H_2O, and a strong deviation from linear degassing of CO_2. This likely reflects Fuego's significantly higher H_2O/CO_2 ratio compared to all other basalts. Mixed-volatile solubility experiments have revealed non-ideal mixing behavior in H_2O–CO_2 fluids, with the effect compounded at pressures above 5000 bars [Botcharnikov et al. 2005; Behrens et al. 2009; Lesne et al. 2011b; Iacovino et al. 2013].

For Fuego and Fogo, the depth of degassing of sulfur is highly variable between models, and trends are not consistent between the two basalts. For Fuego, D-Compress (IM) and VolFe predict the onset of significant S degassing at the most shallow depths, but for Fogo they predict the deepest. Sulfur_X and EVo are in the middle of degassing depth estimates for Fuego but predict the most shallow depths for Fogo. Given the strong interconnection between sulfur degassing and the evolution of the oxidation state of the liquid and fluid phases, perhaps that is driving the disconnect. The implementation of sulfur modeling in each tool involves choices of multiple interconnected models, resulting in significant divergence for the modeled behavior of S and fO_2 during degassing. Fuego's high H_2O concentration of 4.5 wt% may also contribute, since the increased abundance of H can, along with fO_2, affect the activity of H_2S relative to SO_2 in the fluid (and in the case of D-Compress, in the melt). Fuego is also significantly more evolved than Fogo.

3.3 Magma redox: oxygen fugacity and sulfur and iron speciation in the melt

Across the full degassing path, all models disagree significantly for all redox variables (Figure 4), which were input as $Fe^{3+}/\Sigma Fe$ for MORB, Kīlauea, and Fuego but as ΔNNO for Fogo. The large disagreement in initial fO_2 reflects how seemingly subtle model assumptions greatly affect results, consistent with the range of methodologies employed for calculating and translating between redox variables (see Supplement). The modeled $Fe^{3+}/\Sigma Fe$ for Fogo exemplifies this; the starting values at P/P_i=1 range from relatively reduced around 0.2 (D-Compress) to oxidized around 0.4 (MAGEC). These models diverge even further as pressure drops, with $Fe^{3+}/\Sigma Fe$ spanning 0.1 to 0.5. The strong mismatch in modeled $S^{6+}/\Sigma S$ for D-Compress likely reflects different reaction mechanisms. D-Compress models S in the melt as SO_2 (S^{4+}) and H_2S melt species, while the other tools model S melt species as S^{6+} and S^{2-} (see discussion).

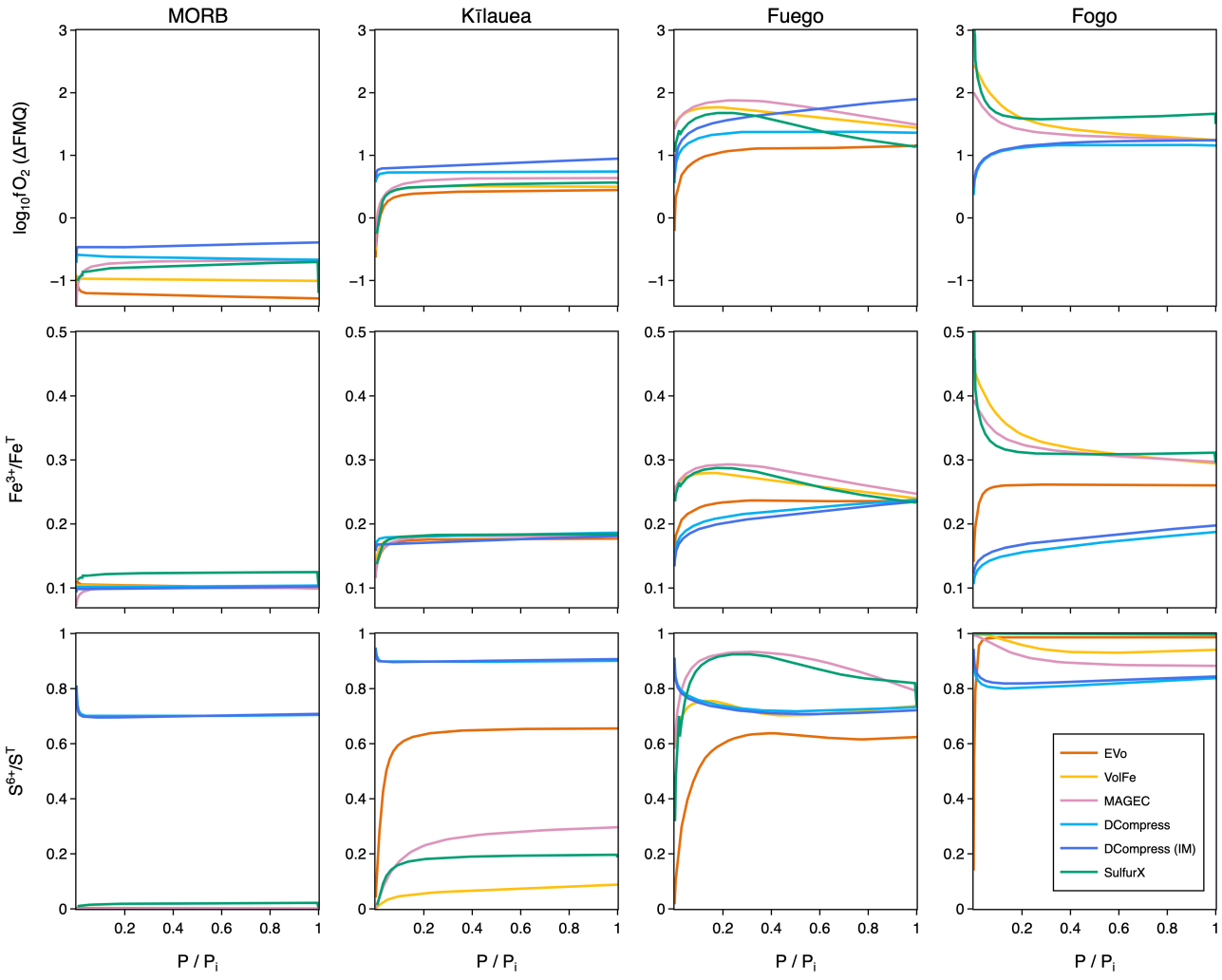

Figure 4: Degassing simulations with all tools for all basalts showing the change in oxygen fugacity relative to the FMQ buffer, iron redox, and sulfur redox as a function of pressure during degassing. For all models except D-Compress, the $S^{6+}/\Sigma S$ is essentially zero for MORB.

Tools show the smallest deviation in Fe speciation, modest deviation in fO_2 (as ΔFMQ), and extreme deviation spanning nearly a factor of 3 (a factor of 4 including D-Compress) for sulfur speciation. All tools predict steady redox values during degassing until low P, also reflected in the P of the onset of appreciable sulfur degassing (Figure 3). In all cases, the very end stages of degassing at the lowest P are where all tools predict the largest changes in redox variables, where both S and H are degassing appreciably. Fogo degassing runs show that tools are split on the change in slope of redox evolution at low pressure. EVo and D-Compress predict more reducing conditions at shallow depths, consistent with their predictions for the other three basalts, where MAGEC, VolFe, and Sulfur_X all predict increasingly oxidizing conditions below P/P_i=0.1.

3.4 Vapor composition

Figure 5 shows the modeled values for molar C/S^v and $\log(SO_2/H_2S)^v$ for each system. Vapor composition at the vent (at atmospheric pressure in our runs) is the ultimate model output where large inter-tool variations in volatile speciation are expected. All models consistently predict decreasing C/S^v with decompression, converging to near unity at surface pressure,

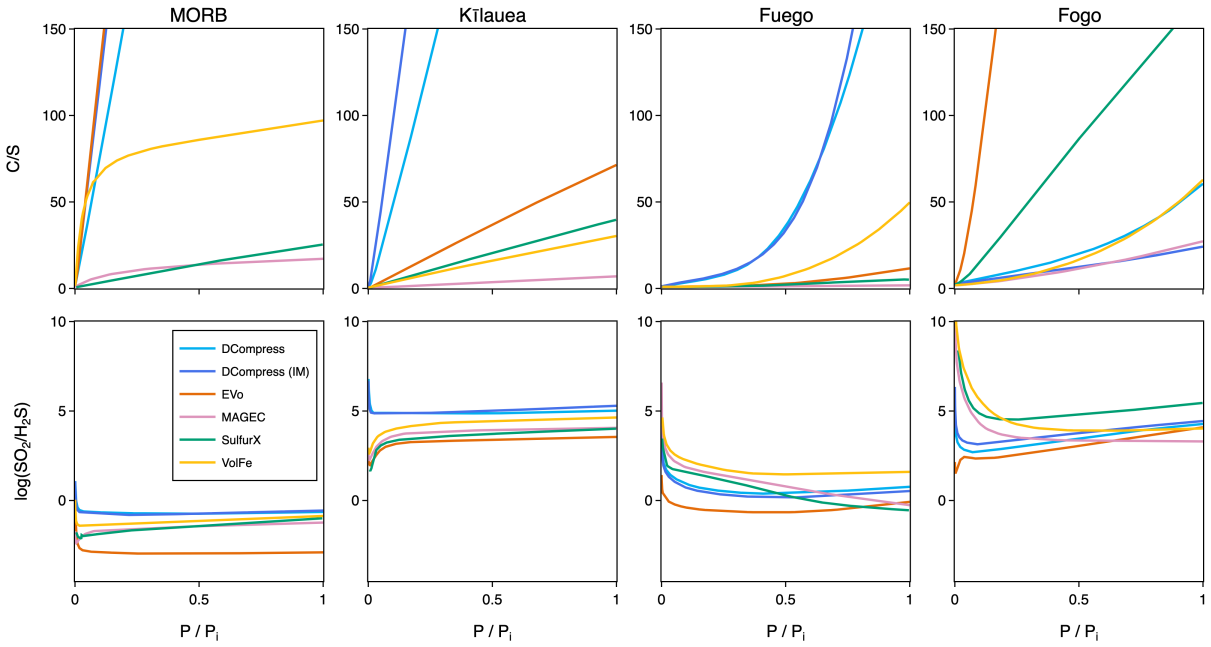

Figure 5: Calculated values of C/S and log(SO_2/H_2S) molar ratios in the vapor phase as a function of normalized pressure of degassing for each volcanic system.

consistent with their canonical degassing behaviors, but this is driven by the strong differences in degassing behavior of these two species and does not imply good model agreement in calculated vapor composition at low pressures. Substantial inter-model variability exists across all basalts, with the magnitude of disagreement strongly dependent on bulk melt composition.

The normalized pressure of the onset of S degassing as shown in Figure 3 generally maps to C/S^v where deeper S degassing results in consistently lower C/S^v across the entire pressure range. In Figure 2, computed P^v_{sat} for MORB and Kīlauea deceptively appear to be in better agreement than those of Fuego and Fogo due to the shared y-axis, but relative model disagreement is similar across all systems. Normalizing for variable P^v_{sat} values, models show much better agreement for volatile-rich compared to volatile-poor systems. A larger absolute pressure range of degassing may explain this discrepancy.

Trends in modeled log(SO_2/H_2S)^v between P/P_i=1 and ~0.1 (or 1 and ~0.25 for Fogo) are very consistent, but all models strongly diverge growing discronant at low (near-vent) pressures. The actual values for SO_2/H_2S are likewise in stark disagreement. Note that the SO_2/H_2S ratio is plotted in Figure 5 in terms of $\log_{10}$; models disagree by several orders of magnitude. On top of the variability in modeled P^v_{sat} and onset of S degassing, SO_2/H_2S is directly reflective of redox evolution and all of the parameterizations and modeling choices made by each tool driving it.

Figure 6 shows the calculated volcanic gas compositions in weight fraction at 1 bar. The species with the most inter-tool variability is H_2S, which is a consequence of the strong variations of the dissolved sulfur and S speciation during ascent. Overall, the Fuego composition yields the most consistent gas composition among the tools and the MORB composition yields the most variable gas composition.

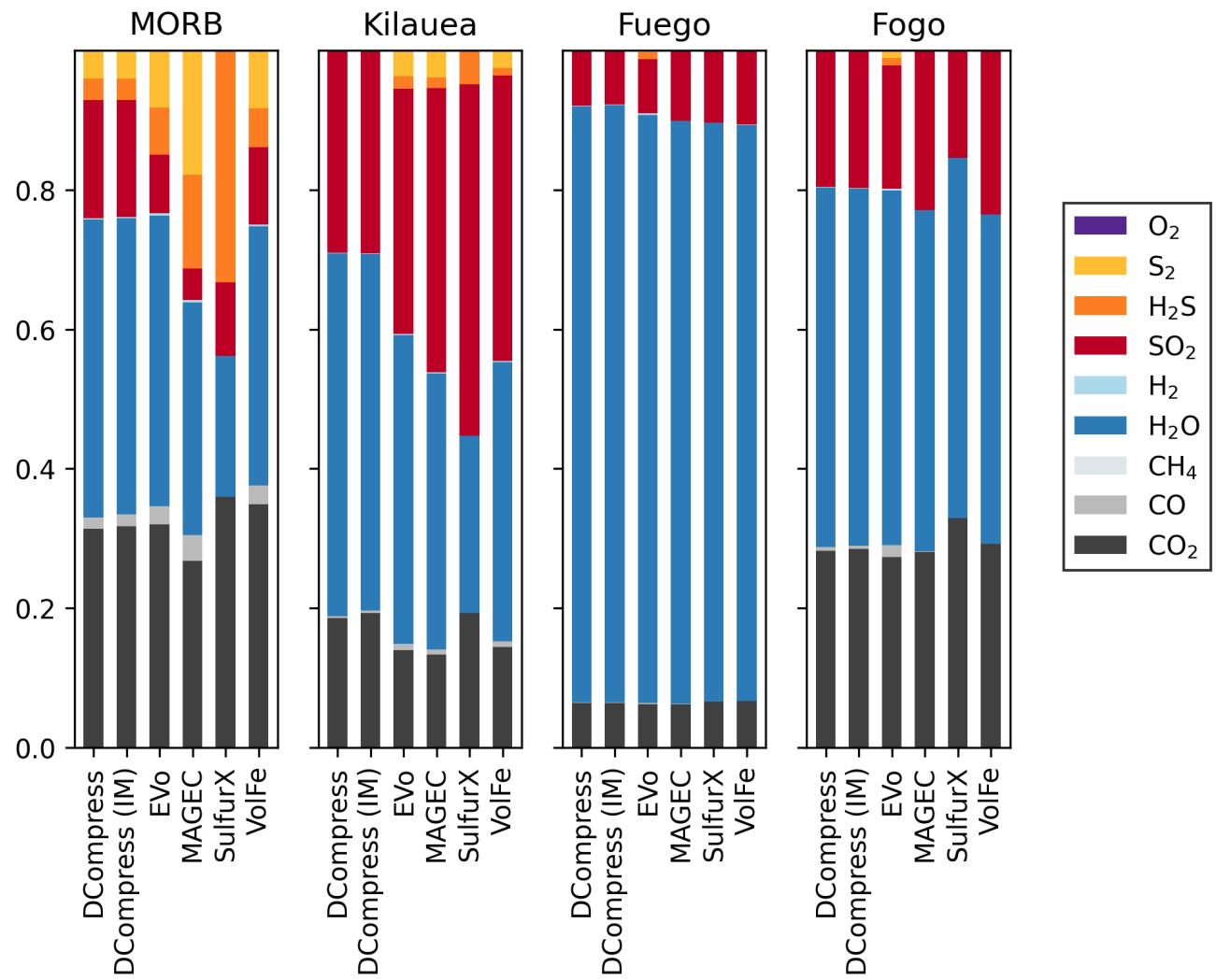

Figure 6: Species weight fraction in the vapor phase calculated at atmospheric pressure with each tool for all four basaltic systems.

4 Discussion

4.1 Differing volatile 'solubilities' between models and tools

Given the large variety of model parameterizations in each tool, it is challenging to isolate specific drivers of significant variability in tool outputs. Here we examine differences in how tools implement volatile solubility laws, where we define solubility as the concentration of a particular volatile species in the melt at a given P, T, melt composition, and fO_2. We can consider two aspects driving the starkly different results observed between tools, which will result in differing volatile solubilities: tool implementation and model parameterization. The former includes the choice of internal model equations (e.g., for redox conversions), vapor-melt reactions, intrinsic assumptions, mathematical solvers, and even typos or errors. Included in the model parameterization is the choice of the thermodynamic equation describing vapor-melt reactions and the empirical constants applied to that equation. That means that even for tools using the same vapor-melt reactions and equation forms, the

experimental data and methodology used to regress its constants are what define a model's uniqueness in the most fundamental sense. In the following sections, we take a thermodynamic approach to try and untangle these differences.

Based on melt–vapor reactions for different volatile species, we can calculate a proportionality factor (H_i'), which has the following generic form and can be calculated simply from calculation outputs:

$$H_i' = \frac{\left(w_i^m\right)^n \left(fO_2\right)^m}{x_j^v P} \tag{15}$$

where w_i^m is the weight fraction of species i in the melt, x_j^v is the mole fraction of species j in the vapor, and n and m are the stoichiometric exponents for the volatile species i and fO_2 based on the vapor-melt reaction. We compare H_i' for the main volatile species in our calculations: total H_2O, total CO_2, and reduced and oxidized S. Given most tools use IM, we use their melt–vapor reactions for H_2O (combining their eq. 8 and 9) and CO_2 (their eq. 1). Therefore, for H_2O solubility, i = total H_2O, j = H_2O^{vapor}, n = 2, and m = 0 ($O_2(v)$ is not involved in the melt–vapor reaction). Similarly for CO_2, i = total CO_2, j = CO_2^{vapor}, n = 1, and m = 0. For reduced S (S^{red}), given all tools except for D-Compress assume eq. 2 or an equivalent reaction, i = S^{red}, j = SO_2^{vapor}, n = 1, and m = 1.5 ($O_2(v)$ is involved in the melt–vapor reaction). Similarly, for oxidized S (S^{ox}), we use eq. 6 as the base: i = S^{ox}, j = SO_2^{vapor}, n = 1, and m = -0.5.

The proportionality factor is the combination of the equilibrium constant/solubility function/capacity (we refer to all of these as a solubility function during this discussion for simplicity), which is typically a function of P, T, and melt composition (sometimes including H_2O); and the fugacity coefficient (γ_i), which is a function of P and T (all these tools treat the vapor as an ideal mixture of non-ideal gases and hence γ_i does not depend on vapor composition). By construction, H_i' is intended to remove the explicit dependence on fO_2, vapor composition, and the CO_2 and S content of the melt, allowing us to compare the effective solubility functions implied by each tool. This diagnostic is most direct for H_2O and CO_2. For sulfur, however, $H'_{S^{red}}$ and $H'_{S^{ox}}$ should not be interpreted as isolated sulfur-solubility laws, because the assumed melt–vapor reaction, Fe-redox conversion, sulfur speciation model, and treatment of sulfur-bearing phases differ among tools. This caveat is particularly important for MAGEC, where Fe redox, fO_2, and S redox are solved as coupled parts of the gas-melt equilibrium framework. An example of H_i' calculated for Fuego model runs is shown in Figure 7, with figures for the other compositions shown in the Supplementary Material. The calculated H_i' values are plotted as a function of P as H_i' are expected to vary with P because both solubility functions and γ_i's depend on P. The larger the value of H_i', the more of that volatile species can dissolve in the melt at a given set of conditions. If the tools predicted the same volatile solubility at a given set of conditions, curves of H_i' vs. P would be the same for all tools for each calculation. However, H_i' varies greatly between tools. So what is driving these variations?

Firstly, H_i' depends on γ_i. All tools use the same or similar parameterizations for γ_{SO_2} [Shi and Saxena 1992; Hughes et al. 2023] and γ_{CO_2} [Holland and Powell 1991; Shi and Saxena 1992], and their independent implementations give similar results (see Supplement). A wider variety of parameterizations for γ_{H_2O} are used [Peng and Robinson 1976; Holland and Powell 1991; Shi and Saxena 1992], which could account for some of the variation in H'_{H_2O}, but is likely to be a small component. Overall, variations in γ_i are unlikely to be the main driver of variations in H_i'.

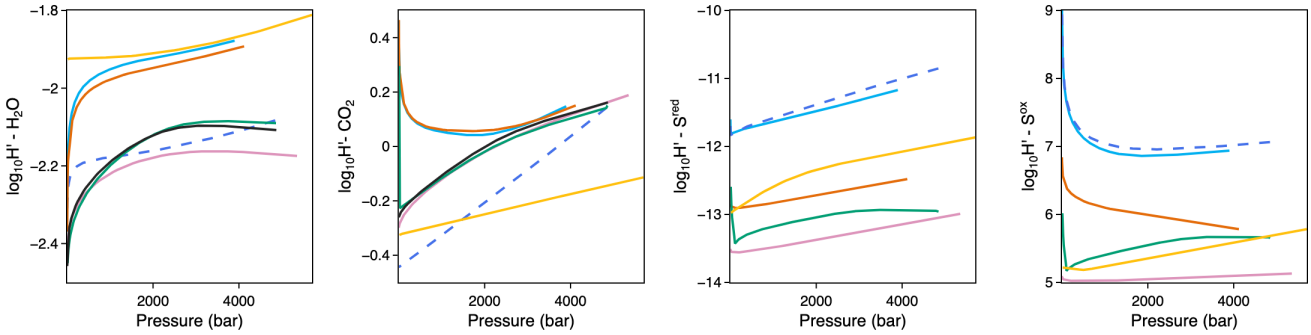

Figure 7: Volatile proportionality factors (eq. 15) with all tools for Fuego basalt showing the change in H_2O, CO_2, reduced S (S^{red}), and oxidized S (S^{ox}) proportionality factors (H_i') as a function of pressure during degassing.

This leaves the solubility functions, which depend on P, T, and melt composition and are highly varied between tools. For H_2O and CO_2, tools fall into one of three groups: those that use IM (D-Compress (IM), MAGEC, Sulfur_X, VESIcal (IM)); those that use D-Compress (D-Compress, EVo); and VolFe, which uses Hughes et al. [2024a]. These groupings are mostly reflected in values of H'_{H_2O} and H'_{CO_2} as shown in Figure 7. Differences in H_2O and CO_2 solubility are the main causes in the differences in P^v_{sat} (Figure 2). VolFe predicts the lowest CO_2 solubility (H'_{CO_2}) and the highest P^v_{sat} for Fuego; all other tools have similar CO_2 solubilities at P^v_{sat} and their order in P^v_{sat} is thus governed by their H_2O solubilities, with EVo/D-C having high H_2O solubilities and therefore lowest P^v_{sat}. The different groupings of models predict different H_2O and CO_2 solubility for the same melt composition and T and can also be influenced by the H_2O content of the melt for IM. The presence of additional reduced vapor species (H_2, CO, and CH_4) will have an additional effect on P^v_{sat}. Given the oxidized conditions of these calculations, this will be minor, but could be important in extraterrestrial applications [Hughes et al. 2024b].

The proportionality factors for both reduced and oxidized sulfur vary by multiple orders of magnitude across tools (Figure 7). Unlike H'_{H_2O} and H'_{CO_2}, which broadly reflect the H_2O–CO_2 solubility-model groupings described above, the sulfur proportionality factors fold together sulfur solubility/capacity terms, melt–vapor reaction choices, Fe-redox conversions, and S-redox models. Therefore, H'_{Sred} and H'_{Sox} should be interpreted as effective tool-level sulfur behavior rather than isolated sulfur-solubility laws. This coupled behavior is consistent with the wide range of S degassing paths shown in Figure 3. For Fuego, D-Compress has the largest H'_{Sred} and H'_{Sox}, which means sulfur is more soluble in the melt, causing sulfur to remain in the melt to shallower depths than the other tools (Figure 3). MAGEC plots at the low end of both sulfur proportionality factors; however, this should not be attributed to sulfur solubility alone. MAGEC's distinct sulfur-degassing behavior likely reflects the coupled effect of its Fe- and S-redox models, in which the Fe-redox-derived fO_2 propagates through sulfur speciation and into the predicted degassing path.

4.2 Intrinsic assumptions and hidden variables: Redox and sulfur

The complicated web of nested, interconnected assumptions made by mixed-volatile modeling tools can perhaps best be exemplified by how each tool handles redox. The very concept of *oxygen fugacity* in the context of magmatic systems is a universal pain point among petrologists, especially when attempting to communicate or compare results across studies, let alone across disciplines. Researchers commonly express the redox state of a system in terms of: 1. oxygen fugacity, fO_2,

relative to a buffer (e.g., ΔNNO+1); 2. the numerical value for fO_2 (e.g., $\log fO_2$ = -12); or 3. the ratio of valence states of Fe or S (e.g., $Fe^{3+}/\Sigma Fe$ or $S^{6+}/\Sigma S$). "Translating" between representations requires the use of models to do so. Not only is there a level of disagreement between such models, but they are applied in various ways (sometimes incorrectly) in the literature. For example, the numerical fO_2 value of a buffer is dependent upon P. It is common to disregard this P term (assuming P = 1 bar), which may be a reasonable simplification at low P but causes larger errors as P increases. The lack of consensus on the definition of each buffer value at any given P and T is a well recognized problem in the igneous petrology community [Anenburg and O'Neill 2019; Wieser and Gleeson 2023].

Consider a scenario in which we measure the concentration of both FeO and Fe_2O_3 in a silicate melt such that $Fe^{3+}/\Sigma Fe$ = 0.5. To input redox into a modeling tool, we must translate this measured value into a form that that tool can accept. EVo, MAGEC, and VolFe can accept $Fe^{3+}/\Sigma Fe$ value directly. D-Compress only accepts redox referenced to the NNO redox buffer, and Sulfur_X only to the FMQ buffer. Before we can calculate fO_2 referenced to a buffer, we must first convert $Fe^{3+}/\Sigma Fe$ into a value for the activity of oxygen in the melt (typically assumed equal to fO_2). Most tools rely on the model of Kress and Carmichael [1991] except for MAGEC, which implements its in-house model [Sun and Yao 2024]. A subtle but important detail is that VolFe uses the equation from the appendix of Kress and Carmichael [1991, eqs. A-5 and A-6] while the others use the version in the main text (eq. 7). This results in small but nontrivial discrepancies in the oxygen activities, but as additional modeling choices are made, this divergence compounds. For instance, the initial fO_2 values computed by our tools vary over an order of magnitude in all basalts (Figure 4).

An additional complication comes from the fact that the Kress and Carmichael [1991] paper only considers anhydrous compositions, so there is ambiguity as to whether these equations should be implemented with hydrous cations as in rhyoliteMELTS [Ghiorso and Gualda 2015] and D-Compress, or anhydrous cations as in EVo and VolFe. Although the effect on Fe speciation is relatively small (e.g., for the Fuego composition, $Fe^{3+}/\Sigma Fe$ changes by 2.6% from 0-8 wt% H_2O), this can have a significantly larger effect on the calculated S speciation given its rapid shifts with Fe speciation, around 30% for the model of Nash et al. [2019].

Next, our redox value goes through another model filter: how the equilibrium state of a buffer assemblage is defined. There are several published derivations or recalibrations of redox buffer equations. As new data have emerged, these formulations have evolved to extend to higher P and T, reduce uncertainties, or correct past errors. The result is a vast array of publications throughout the literature spanning several decades. Model developers must therefore choose not only which formulation to use, but how to apply it; for example, whether to include P corrections or adopt specific activity models. The cumulative effect is an overwhelming set of permutations of possible assumptions embedded in the seemingly "simple" act of quantifying a magma's redox state.

In most of our calculations, we specified $Fe^{3+}/\Sigma Fe$ as the redox variable, and its conversion to fO_2 depends on P: at 5000 bar, all iron speciation models used in these tools predict fO_2 values ~0.5 log units higher than those calculated at 1 bar for the same $Fe^{3+}/\Sigma Fe$. This means the initial fO_2 when calculated from $Fe^{3+}/\Sigma Fe$ varies significantly at P^v_{sat} due to both the different iron speciation models used but also the different P due to the differences in mostly H_2O–CO_2 solubility. Even accounting for the effect of P, no tools predict the same $Fe^{3+}/\Sigma Fe$ at a given fO_2, and the same is true for $S^{6+}/\Sigma S$, highlighting

that different parameterizations and their independent implementations results in variations in calculated values. This sets the stage for different evolutions of melt S, melt $S^{6+}/\Sigma S$, and fO_2 during degassing.

D-Compress predicts a different relationship between S^{ox}/S^{red} and fO_2 because it assumes different reaction mechanisms for both reduced and oxidized sulfur (it depends on f_{SO2} and f_{H2S}). The assumption of SO_2 and H_2S as the dissolved sulfur species in D-Compress leads to a different expected redox evolution because SO_2 has a different sulfur oxidation state (4^+) to sulfate (6^+), as assumed in the other tools.

4.3 Typos, normalization, and the importance of benchmarking

VESIcal is a unified implementation of several pre-existing models as opposed to other models examined here, which likewise implement several existing models (e.g., for H_2O solubility) but couple these to their own new model (e.g., for S behavior). In the development of VESIcal [Iacovino et al. 2021; Wieser et al. 2022], the authors built benchmark testing routines to ensure that each model implemented reproduced the original publication's datasets. Although demonstrating the veracity of a new model is established practice in our field, benchmarking implemented existing models is not, nor is it one that manuscript reviewers are looking for. Given tools are independently implementing the same models, benchmarking is critical to ensure that results are comparable.

Even simple model equations can have hidden issues. Iacovino et al. [2021] documented a typo in the H_2O–CO_2 model of Iacono-Marziano. The equation for carbon is written as a calculation of CO_3 solubility, but the equation is actually for CO_2 solubility. Given the model is for mafic magmas, where carbon is complexed in the melt as CO_3, it would be reasonable for the equation to express carbonate solubility instead giving little reason for a reader to question it. In its original form, Sulfur_X assumed the equation was for CO_3, and converted this output into CO_2. This resulted in CO_2 solubility estimates that were ~1.36× the true value (the ratio of the molar mass of CO_2/CO_3 = 44/60), leading to anomalously high P^v_{sat} estimates (factor of ~2×) . Sulfur_X was fixed early after publication. Similarly, the published Duan and Zhang [2006] H_2O–CO_2 EOS contained errors in the equations for the partial fugacity coefficient [Yoshimura 2023] that would have caused similar issues had it been incorporated into solubility models. Models within a tool should be benchmarked against existing tools (i.e. the Iacono-Marziano web app) prior to publication, and tool output should be compared to known values from experiments or direct measurements. Through benchmark testing, the authors of VESIcal also discovered that even seemingly innocuous decisions such as the choice of normalization routine can cause testing against original publications to fail with errors of several percent relative [Iacovino et al. 2021].

4.4 Compounded variability in modeled vapor composition

Vapor composition is arguably the most important model output for volcano observatories who measure active volcanic gas compositions for forecasting eruptive behavior [Aiuppa et al. 2007; De Moor et al. 2016; Kern et al. 2022]. The ratio of C to S in volcanic surface gases is a useful indicator of the depth of the source of gas, since C degases relatively deep and S relatively shallow, and H is difficult to measure [Giggenbach 1996; Aiuppa et al. 2007; Burton et al. 2007; Iacovino 2015; De Moor et al. 2016; Kern et al. 2022; Ding et al. 2025]. High C/S can indicate the addition of new magma into the deeper part of the magma chamber [Aiuppa et al. 2007; De Moor et al. 2016; Ding et al. 2025]. This added heat and often added volatiles can result in

eruption at the surface. C/S can also be used to monitor fluctuation in the interaction between the magma and a hydrothermal system, since SO_2 is highly soluble in water where carbon is not [De Moor et al. 2016; de Moor et al. 2016; Stix and de Moor 2018].

The variation in C/S^v (Figure 5) is significantly larger than that in dissolved melt volatiles (Figure 3). This is due to a compounding effect, where layer upon layer of model choices stands between the description of dissolved volatiles (derived directly from measured initial concentrations) and the composition of the vapor phase. This includes several equations and constants required to describe melt-vapor equilibrium such as fugacity coefficients, homogeneous vapor equilibria, solubilities, and redox behaviors. For instance, mole fraction of a vapor species (x_i^v), its fugacity (f_i), and its partial pressure (p_i) are related according to:

$$x_i^v = f_i/(\gamma_i P) = p_i/P. \tag{16}$$

Where P is the total pressure and γ_i is the fugacity coefficient. So, even if the same f_i is predicted at a given volatile content (i.e., the same solubility), if P or γ_i is different a different x_i^v will be calculated.

The tools include different formulations for calculating homogeneous vapor equilibrium constants (D-Compress and VolFe use Ohmoto and Kerrick [1977]; EVo and MAGEC use in-house versions based on NIST/JANAF databases; and Sulfur_X only includes H_2S-SO_2) and are within ± 0.1 $\log_{10}$ (~16%) of each other for all such equilibrium constants (see Supplement; EVo-RTD* Figure 6). These seemingly small differences can lead to ≤5% differences in the molar concentration of most vapor species, and ≤10% for SO_2 (EVo-RTD Figure 7), contributing to variations in calculated vapor compositions.

Additionally, reduced C and H species including H_2, CO, and CH_4 become dominant at redox conditions more reducing than those typical in terrestrial volcanic systems [~IW < 1; Holloway and Blank 1994] but can be present at mol% concentration even in more oxidizing Earth systems. All tools apart from Sulfur_X and VESIcal consider reduced species in the melt and vapor. In our degassing scenarios, CO is predicted to be 5–12 mol% of the vapor for much of the MORB degassing path and 2–4 mol% for Kīlauea (Figure 6). For the oxidized conditions of Fuego and Fogo, CO is negligible (H_2 is a trace, and CH_4 is negligible for all the conditions explored here; Supplementary Material). Carbonyl sulfide (OCS) can become a minor vapor species at low fO_2 and is currently only included in VolFe and MAGEC (and EVo and D-Compress at 1 bar; Supplementary Material). Therefore, if reduced species are expected to be significant in the vapor and/or melt as in lunar magmas, additional consideration is required to justify the use of a particular model.

Ultimately, the solubilities in these tools are not the same – and the models for C and S are highly divergent – making the C/S^v particularly sensitive to differing solubilities. Even a 20% relative difference in the predicted $x^v_{CO_2}$ and $x^v_{S_T}$ – but in opposite directions – can quickly lead to 60–150% differences in C/S^v. Given the sensitivity of sulfur solubility to fO_2 and sulfur speciation, both of which vary between tools, these coupled redox-solubility choices add to the variability in vapor composition. This is partly because the vapor composition is very different from the melt composition: there is a long lever connecting the melt and vapor compositions, and therefore small changes to the volatile melt composition result in large changes to the coexisting vapor composition.

*https://EVo-outgas.readthedocs.io/en/latest/EVo_doc.html#benchmarking

We illustrate the consequences of the inter-tool variability of vapor composition by using such outputs to recover the total amount of gas emitted at the vent. The ratio of the emission rate (generally in t/day) of all the gas species, Q_T, and that measured for SO_2, Q_{SO_2}, is:

$$\frac{Q_{SO_2}}{Q_T} = \frac{w^v_{SO_2}}{w^v_T} \tag{17}$$

where $w^v_{SO_2}$ is the weight fraction of SO_2 in the vapor and $w^v_T = 1$ is the total weight fraction of the vapor species. Thus, total amount of gas emitted at the vent can be obtained by multiplying the measured SO_2 flux by the inverse of the SO_2 weight fraction predicted by the tools. The total gas flux varies the most for the MORB composition, the highest flux being 3.7 times higher than the lowest flux ($1/w^v_{SO_2}$ of MAGEC is 3.7 times higher than that of D-Compress in Figure 6). The maximum difference between the tools for all the other cases is ≈ 40%. Combined with the intrinsic uncertainty of SO_2 flux measurements, we estimate that using tool outputs to estimate total gas fluxes is only precise to within one order of magnitude.

Vapor composition is difficult to measure experimentally and thus is very rarely undertaken eggler1979solubility-b9e, holloway1986, jakobsson1986, taylor1989, pawley1992, jakobsson1994, iacovino2013, o2002sulfide,Oneill2022,gorojovsky2026solubility,boulliu Even more rare is a solubility model regressed using these data. The best example of this is perhaps Moore et al. [1998], whose model for H_2O up to 3 kbar is robust but underutilized by studies looking to interpret melt inclusion data since fH_2O is rarely if ever known. Similarly, sulfide and sulfate capacity models require knowledge of fO_2 and fS_2 or fSO_2, which are difficult to independently constrain in natural systems [O'Neill 2021; Boulliung and Wood 2022; O'Neill and Mavrogenes 2022; Boulliung and Wood 2023; Gorojovsky and Wood 2026; Thomas and Wood 2026]. The relationship describing equilibrium at the melt–vapor interface, however, is critical for modeling and underpins most tools, which thermodynamically calculate fugacity values. Solubility experiments that directly measure the vapor phase, while challenging, represent a path to significantly improving the application of degassing models to observatory science by quantifying the relationship between the fugacity of a volatile in the vapor and its activity in the melt.

5 Future directions

5.1 Tips for users

The biggest challenge for scientists that wish to implement models from the literature is in deciding which model(s) or tool(s) to use. It is critical that the choice of modeling tool be well justified when presenting model results. Here are some actionable recommendations for effectively doing so:

1. **The model should consider reactions appropriate to system conditions.** Just because a tool will allow users to model a particular scenario does not imply that it will produce sensible results. Lunar magmas are more reducing than terrestrial ones to the point that reduced melt and vapor species become important [Scaillet and Pichavant 2004; Newcombe et al. 2017]. Sulfur_X and all VESIcal sub-models (including Iacono-Marziano, which is commonly used in extraterrestrial applications) do not consider reduced species.

2. **The magma composition should fall within the model's calibration dataset.** While it is difficult to untangle precisely the *P-T*-composition space any model is appropriate for [Iacovino et al. 2021], a user can make an informed decision by examining the experiments used to calibrate the model. VESIcal and PySulfSat both implement simple methods for the user to do so. CO_2 and both reduced and oxidized sulfur solubility are incredibly dependent on melt composition [O'Neill and Mavrogenes 2002; Ghiorso and Gualda 2015; O'Neill and Mavrogenes 2022], so care must be taken that the underlying models used for these parameters are appropriate for your system.

3. **Check model results against measured values if available.** If any measured data are available for your system or one very much like it, a good test of model applicability is to compare model outputs against known results. For example, does the model accurately reproduce experimental saturation pressures? How about measured $Fe^{3+}/\Sigma Fe$ and $S^{6+}/\Sigma S$ in experiments and/or MI? Or measured $SO_2/(SO_2+CO_2)$ in FI with P from CO_2 density?

Calculations performed by users should follow FAIR guidelines: the version of the code should be included; model options used within the tool should be clearly recorded and cited appropriately; and a notebook or script to recreate the calculations and all model results should be included as supplementary material. We have provided an example of how to properly justify and cite a model in a manuscript in the Supplementary Material.

5.2 Tips for model authors

Moving forward, several steps can be taken by individual scientists to make our model space cohesive, transparent, and interoperable:

1. **Improved documentation.** Docstrings should be used within code to document the arguments, variable units, and output types of all functions. Code should be made publicly available on accepted repositories such as GitHub, following FAIR [Wilkinson et al. 2016] guidelines. Stating that the code is available upon request is not acceptable in a peer-reviewed manuscript. At a minimum, a README file should provide a minimum working example of the functionality of the model code. Ideally, a dedicated documentation website (e.g., via ReadTheDocs) would be provided with several worked examples. An open-source license file should also be included in the repository. The version of the code used for the publication of a manuscript must be archived with a version number and ideally assigned a DOI (e.g., via Zenodo) such that the manuscript results can be reproduced in perpetuity.

2. **Libraries over scripts.** A single script that an end-user can edit and re-run is a reasonable starting point for tools with relatively low complexity but is difficult to integrate with other modeling workflows. A code library consisting of discrete functions allows users to use, combine, and iterate over calculations. Moreover, it would drastically improve our ability to compare tool functionality while at the same time enabling multiple tools to use the exact same implementation as one another (e.g., VolFe uses PySulfSat's implementation of many models). For example, a single well-documented and bench-marked function for converting between iron redox state and fO_2 with eq. (7) of Kress and Carmichael [1991] used by all tools in this work would have eliminated one point of hidden variability leading to divergence in outputs.

3. **Benchmarks and unit tests.** A substantial amount of code within our suite of tools is not bench-marked against expected results or to verify correct implementation of existing model equations. VESIcal provides detailed benchmarks for

all models against the values and figures in the original publications and so IM and VC models within VESIcal were used to benchmark results from our comparative degassing simulations. In their documentation, EVo and VolFe both provide clear outlines of how their benchmarks were performed and provide Jupyter notebooks illustrating their performance.

4. **Model/tool validity limits and intrinsic uncertainty.** Most published models are based on experimental datasets that have well-known P, T, and melt compositions. Some, such as the IM model, use a compilation of experimental studies, which complicates the definition of a validity range. This is especially true when the hull of the multidimensional parameter space is non-convex or has holes. For example, D-Compress solubility relationships are calibrated for basaltic and rhyolitic melts but lack a relationship for dacitic melts. Sometimes, a model's calibration dataset is not explicitly available, which makes it incredibly difficult to evaluate validity limits and uncertainty. The intrinsic uncertainties of models and tools are affected by the same considerations, except that the intrinsic error of tools can be estimated in at least two ways. The first method is to adopt a Monte-Carlo approach by running multiple realizations with perturbed initial conditions and characterize the envelope of the outputs as in Hughes and Saper [pre-print]. The second method is to compound the intrinsic errors of all the relevant models used within a given tool to yield a consolidated intrinsic error of a given output of that tool as in Burgisser et al. [2015].

5. **Community standards and governance.** An agreed upon set of standards for how codes are built would provide a perpetual framework not only for bridging existing tools but for enabling new tools to easily enhance or slot into the existing peer-reviewed literature. Moreover, it provides end-users with a common model language. For example, the community could agree on a format for documenting the units of all values used in their tool, such that a user can easily determine how their data must be input and what results are output. We might require that a developer include this in docstrings and in a table or list on a README or documentation page for the code to be suitable for peer-reviewed publication. We are aware that software longevity is contingent on the evolution of programming languages and platforms and that libraries require continued updating to avoid dependency issues. Community governance documents such as a Code of Conduct, designated leadership roles, and points of contact are standard requirements for scientific Python organizations such as NumFOCUS and PyOpenSci. A community-governed ecosystem would define best practices for writing and distributing volcano geochemistry model code. Its leadership would provide a communication platform, interaction pathways, and contribution guidelines and would set requirements for documentation and testing. Such maintenance requires an active community dedicating time and resources to avoid tool obsolescence. This is challenging given that academic "credit" is not given to those who spend additional time properly documenting their code, contributing to code maintenance, or reviving non-operational code created by another research team. For tenure-track faculty, these practices are often explicitly discouraged, and very few mechanisms exist to fund such work.

6 Conclusions

We performed matching magma degassing calculations on mid-ocean ridge, Kīlauea, Fuego, and Fogo basalts using our own published modeling tools: D-Compress [Burgisser et al. 2015], EVo [Liggins et al. 2020; 2022], MAGEC [Sun and Lee 2022; Sun and Yao 2024], Sulfur_X [Ding et al. 2023], VolFe [Hughes et al. 2024a; Hughes et al. 2025], and implementations of VolatileCalc [Newman and Lowenstern 2002], Iacono-Marziano [Iacono-Marziano et al. 2012], and MagmaSat [Ghiorso and Gualda 2015]

within VESIcal [Iacovino et al. 2021]. We have shown the clear variability in modeling tool outputs for a range of basalts. We speculate that differences when modeling andesites and rhyolites would be at least as variable, highlighting the caution required when modeling an evolutionary suite of magma compositions. Major findings of this work that can guide the community in improving our tools for academic and operational purposes include:

1. Improved community consensus on the implementation of redox variables like $\log f O_2$, $Fe^{3+}/\Sigma Fe$, $S^{6+}/\Sigma S$, and redox buffer equations is critical to interpreting volcanic sulfur both at the vent and in the rock record.
2. Targeted experiments on SiO_2-poor, alkali-rich basalts like Fogo could significantly improve the accuracy of modeled vapor saturation pressures (and, thus, magma storage depths) of primitive magmas.
3. Sulfur has little to no effect on the calculation of the pressure of vapor saturation when considered in addition to H_2O and CO_2.
4. Community governance is critical to creating agreed-upon standards for modeling, coding, and publishing in volcanology. The points briefly touched on in Section 5 should be turned into a more comprehensive guide, written by the community and enforced during peer review.

Interoperable, data-driven methodologies are required to provide the shared computational language capable of addressing new questions in volcano science. The lack of interoperability inhibits evaluation of model results, obscuring the applicability of a tool to any given scenario and which gaps in our experimental literature are most critically needed to improve model accuracy. Platforms such as VICTOR [Lev et al. 2025] help scientists find and use volcanology computational tools via a centralized, cloud-based platform that allows users to run a multitude of models in the browser, without needing to install any tools locally. This significantly lowers the barrier to entry for the use of individual tools but nonetheless requires significant work by end-users to perform comparisons such as those explored here.

What cannot be overstated is the amount of time and effort that was required to ensure consistency across modeling inputs, model options, and even the format and syntax of tool outputs, despite being the original authors of these codes. This shines a light on what the community already knows: the landscape of volatile solubility models is complex and oftentimes opaque to users. We suggest that the field of magmatic volatiles should focus now on the creation of modern, easy-to-use tools, clever implementation of new model equations or methods, and experimental studies driven not by filling all the gaps but in targeting those that matter most. Achieving this requires a focused volatile modeling consortium to fully codify modeling best practices in a living community that can evolve with our scientific pursuits.

Author Contributions

All authors co-organized the 'Modelling volatile behaviour in magmas' workshop at IAVCEI-2023 in Rotorua, Aotearoa New Zealand, which spurred this comparative effort, in addition to the follow-up workshop at Goldschmidt 2026 in Montreal, Canada. All authors collaborated to determine comparative modeling scenarios and worked over the course of nearly three years to ensure "apples-to-apples" comparisons and scientific rigor of the approach and conclusions. KI, EH, AB, PL, SD, and CS carried out modeling performed with their respective modeling tools, including determination of model options and translation

of input and output variables. KI performed additional model runs to address inconsistencies as flagged by all authors and to update the model runs to the most recent available versions of each tool. PW created Jupyter notebook workflows for interrogating input data and interrogating initial model outputs. GK provided important feedback on manuscript text from the perspective of a model user rather than a tool author. KI, EH and AB created the figure generation pipeline available in the supplementary material. KI developed configuration files for documenting model options as captured in model runs. All authors contributed to the manuscript text.

Acknowledgements

ECH and GK were supported by the New Zealand Ministry of Business, Innovation and Employment (MBIE) through the Hazards and Risk Management (Strategic Science Investment Fund, contract C05X1702); Catalyst Seeding Grant (23-GNS-009-CSG); and MBIE Endeavour Smart Idea (PROP-2104-ENDSI-GNS). PW acknowledges support from a Sloan Research Fellowship. KI thanks A.M.F. Ham for their continued encouragement of this work. All authors thank the speakers and attendees of the 'Modelling volatile behaviour in magmas' workshop at IAVCEI-2023 in Rotorua, Aotearoa New Zealand, and online, globally, for inspiring this work and the follow-up workshop at Goldschmidt-2026 in Montréal, Canada, and online, globally, for getting us on-track.

Data Availability

All data used in this work is available in the Supplementary Material hosted by the journal and on the GitHub repository at: `https://github.com/kaylai/volcanic-gas-modeling-tool-comparison`, including: full datasets used to determine starting compositions and conditions; an example of how starting compositions were chosen from those datasets; all modeling tool outputs; all model options used to generate tool outputs; and Jupyter notebooks to generate every figure in this manuscript.

Copyright notice

References

Acocella, V., M. Ripepe, E. Rivalta, A. Peltier, F. Galetto, and E. Joseph (2024). "Towards scientific forecasting of magmatic eruptions". *Nature Reviews Earth & Environment* 5(1), pages 5–22. DOI: 10.1038/s43017-023-00492-z.

Aiuppa, A., A. Bertagnini, N. Métrich, R. Moretti, A. Di Muro, M. Liuzzo, and G. Tamburello (2010a). "A model of degassing for Stromboli volcano". *Earth and Planetary Science Letters* 295(1-2), pages 195–204. DOI: 10.1016/j.epsl.2010.03.040.

Aiuppa, A., C. Caudron, G. Chiodini, S. Ingebritsen, and F. Viveiros (2025a). "Geochemical Monitoring of Volcanic Fluids in the Twenty-First Century". *Modern Volcano Monitoring*, pages 209–260. DOI: 10.1007/978-3-031-86841-2_8.

Aiuppa, A., M. Agusto, P. Allard, S. Carn, J. M. de Moor, S. Inguaggiato, A. Mazot, Y. Moussallam, and P. Nadeau (2025b). "Geochemical volcano monitoring". *EarthArXiv*. DOI: 10.31223/X5TT6D.

Aiuppa, A., M. Burton, T. Caltabiano, G. Giudice, S. Guerrieri, M. Liuzzo, F. Murè, and G. Salerno (2010b). "Unusually large magmatic CO2 gas emissions prior to a basaltic paroxysm". *Geophysical Research Letters* 37(17). DOI: 10.1029/2010GL043837DigitalObjectIdentifier(DOI).

Aiuppa, A., R. Moretti, C. Federico, G. Giudice, S. Gurrieri, M. Liuzzo, P. Papale, H. Shinohara, and M. Valenza (2007). "Forecasting Etna eruptions by real-time observation of volcanic gas composition". *Geology* 35(12), pages 1115–1118. DOI: 10.1130/G24149A.1.

Allan, J. F., R. Batiza, M. R. Perfit, D. J. Fornari, and R. O. Sack (1989). "Petrology of Lavas from the Lamont Seamount Chain and Adjacent East Pacific Rise, 10° N". *Journal of Petrology* 30(5), pages 1245–1298. DOI: 10.1093/petrology/30.5.1245.

Allard, P., M. Burton, G. Sawyer, and P. Bani (2016). "Degassing dynamics of basaltic lava lake at a top-ranking volatile emitter: Ambrym volcano, Vanuatu arc". *Earth and Planetary Science Letters* 448, pages 69–80. DOI: 10.1016/j.epsl.2016.05.014.

Allison, C. M., K. Roggensack, and A. B. Clarke (2019). "H2O–CO2 solubility in alkali-rich mafic magmas: new experiments at mid-crustal pressures". *Contributions to Mineralogy and Petrology* 174(7), page 58. DOI: 10.1007/s00410-019-1592-4.

— (2022). "MafiCH: a general model for H2O–CO2 solubility in mafic magmas". *Contributions to Mineralogy and Petrology* 177(3), page 40. DOI: 10.1007/s00410-022-01903-y.

Anenburg, M. and H. S. C. O'Neill (2019). "Redox in magmas: Comment on a recent treatment of the Kaiserstuhl volcanics (Braunger et al., Journal of Petrology, 59, 1731–1762, 2018) and some other misconceptions". *Journal of Petrology* 60(9), pages 1825–1832.

Baker, D. R. and R. Moretti (2011). "Modeling the solubility of sulfur in magmas: a 50-year old geochemical challenge". *Reviews in Mineralogy and Geochemistry* 73(1), pages 167–213. DOI: 10.2138/RMG.2011.73.7.

Beermann, O., R. Botcharnikov, F. Holtz, O. Diedrich, and M. Nowak (2011). "Temperature dependence of sulfide and sulfate solubility in olivine-saturated basaltic magmas". *Geochimica et Cosmochimica Acta* 75(23), pages 7612–7631.

Behr, Y., A. Christophersen, and C. Miller (2025). "Probabilistic, multi-sensor eruption forecasting". *Geophysical Research Letters* 52(8), e2024GL112029. DOI: 10.1029/2024GL112029.

Behrens, H., V. Misiti, C. Freda, F. Vetere, R. E. Botcharnikov, and P. Scarlato (2009). "Solubility of H2O and CO2 in ultrapotassic melts at 1200 and 1250 °C and pressure from 50 to 500 MPa". *American Mineralogist* 94(1), pages 105–120. DOI: 10.2138/am.2009.2796.

Botcharnikov, R., M. Freise, F. Holtz, and H. Behrens (2005). "Solubility of C-O-H mixturesin natural melts: new experimental data and application range of recent models". *Annals of Geophysics* 48(4-5). DOI: 10.4401/ag-3224.

Botcharnikov, R. E., R. L. Linnen, M. Wilke, F. Holtz, P. J. Jugo, and J. Berndt (2011). "High gold concentrations in sulphide-bearing magma under oxidizing conditions". *Nature Geoscience* 4(2), pages 112–115. DOI: 10.1038/ngeo1042.

Boulliung, J. and B. J. Wood (2022). "SO2 solubility and degassing behavior in silicate melts". *Geochimica et Cosmochimica Acta* 336, pages 150–164. DOI: 10.1016/j.gca.2022.08.032.

— (2023). "Sulfur oxidation state and solubility in silicate melts". *Contributions to Mineralogy and Petrology* 178(8), page 56. DOI: 10.1007/s00410-023-02033-9.

Bower, D. J., M. A. Thompson, K. Hakim, M. Tian, and P. A. Sossi (2025). "Diversity of Low-mass Planet Atmospheres in the C–H–O–N–S–Cl System with Interior Dissolution, Nonideality, and Condensation: Application to TRAPPIST-1e and Sub-Neptunes". *The Astrophysical Journal* 995(1), page 59. DOI: 10.3847/1538-4357/ae1479.

Burgisser, A., M. Alletti, and B. Scaillet (2015). "Simulating the behavior of volatiles belonging to the C–O–H–S system in silicate melts under magmatic conditions with the software D-Compress". *Computers & Geosciences* 79, pages 1–14. DOI: 10.1016/j.cageo.2015.03.002.

Burton, M., H. Mader, and M. Polacci (2007). "The role of gas percolation in quiescent degassing of persistently active basaltic volcanoes". *Earth and Planetary Science Letters* 264(1-2), pages 46–60. DOI: 10.1016/j.epsl.2007.08.028.

Canil, D. (2002). "Vanadium in peridotites, mantle redox and tectonic environments: Archean to present". *Earth and Planetary Science Letters* 195(1-2), pages 75–90.

Carroll, M. R. and M. J. Rutherford (1988). "Sulfur speciation in hydrous experimental glasses of varying oxidation state; results from measured wavelength shifts of sulfur X-rays". *American Mineralogist* 73(7-8), pages 845–849.

Carroll, M. and M. Rutherford (1985). "Sulfide and sulfate saturation in hydrous silicate melts". *Journal of Geophysical Research: Solid Earth* 90(S02), pages C601–C612.

Christophersen, A., Y. Behr, and C. Miller (2022). "Automated eruption forecasting at frequently active volcanoes using Bayesian networks learned from monitoring data and expert elicitation: application to Mt Ruapehu, Aotearoa, New Zealand". *Frontiers in Earth Science* 10, page 905965. DOI: 10.3389/feart.2022.905965.

Clague, D. A., J. G. Moore, J. E. DIXON, and W. B. Friesen (1995). "Petrology of submarine lavas from Kilauea's Puna Ridge, Hawaii". *Journal of Petrology* 36(2), pages 299–349.

Cottrell, E., S. K. Birner, M. Brounce, F. A. Davis, L. E. Waters, and K. A. Kelley (2021). "Oxygen Fugacity Across Tectonic Settings". In: American Geophysical Union (AGU). Chapter 3, pages 33–61.

De Moor, J. M., A. Aiuppa, G. Avard, H. Wehrmann, N. Dunbar, C. Muller, G. Tamburello, G. Giudice, M. Liuzzo, R. Moretti, et al. (2016). "Turmoil at Turrialba Volcano (Costa Rica): Degassing and eruptive processes inferred from high-frequency gas monitoring". *Journal of Geophysical Research: Solid Earth* 121(8), pages 5761–5775. DOI: 10.1002/2016JB013150.

De Moor, J., A. Aiuppa, J. Pacheco, G. Avard, C. Kern, M. Liuzzo, M. Martinez, G. Giudice, and T. Fischer (2016). "Short-period volcanic gas precursors to phreatic eruptions: Insights from Poás Volcano, Costa Rica". *Earth and Planetary Science Letters* 442, pages 218–227. DOI: 10.1016/j.epsl.2016.02.056.

Denlinger, R. P. and A. Flinders (2022). "Density structure of the island of Hawai'i and the implications for gravity-driven motion of the south flank of Kīlauea Volcano". *Geophysical Journal International* 228(3), pages 1793–1807. DOI: 10.1093/gji/ggab398.

DeVitre, C. L., E. Gazel, R. S. Ramalho, S. Venugopal, M. Steele-MacInnis, J. Hua, C. M. Allison, L. R. Moore, J. C. Carracedo, and B. Monteleone (2023). "Oceanic intraplate explosive eruptions fed directly from the mantle". *Proceedings of the National Academy of Sciences* 120(33), e2302093120.

Ding, S., T. Plank, J. M. de Moor, Y. Moussallam, M. Brounce, and P. Kelly (2025). "Volcanic gases reflect magma stalling and launching depths". *Earth and Planetary Science Letters* 660, page 119349. DOI: 10.1016/j.epsl.2025.119349.

Ding, S., T. Plank, P. J. Wallace, and D. J. Rasmussen (2023). "Sulfur_X: A Model of Sulfur Degassing During Magma Ascent". *Geochemistry, Geophysics, Geosystems* 24(4). DOI: 10.1029/2022gc010552.

Dixon, J. E. (1997). "Degassing of alkalic basalts". *American Mineralogist* 82(3-4), pages 368–378. DOI: 10.2138/am-1997-3-415.

Dixon, J. E., D. A. Clague, and E. M. Stolper (1991). "Degassing history of water, sulfur, and carbon in submarine lavas from Kilauea Volcano, Hawaii". *The Journal of Geology* 99(3), pages 371–394.

Dixon, J. E., E. M. Stolper, and J. R. Holloway (1995). "An Experimental Study of Water and Carbon Dioxide Solubilities in Mid-Ocean Ridge Basaltic Liquids. Part I: Calibration and Solubility Models". *Journal of Petrology*.

Duan, Z. and Z. Zhang (2006). "Equation of state of the H2O, CO2, and H2O–CO2 systems up to 10 GPa and 2573.15 K: Molecular dynamics simulations with ab initio potential surface". *Geochimica et cosmochimica acta* 70(9), pages 2311–2324. DOI: 10.1016/j.gca.2006.02.009.

Fincham, C. J. B. and F. D. Richardson (1954). "The behaviour of sulphur in silicate and aluminate melts". *Proceedings of the Royal Society of London. Series A. Mathematical and Physical Sciences* 223(1152), pages 40–62. DOI: 10.1098/rspa.1954.0099.

Fischer, T. P., G. B. Arehart, N. C. Sturchio, and S. N. Williams (1996). "The relationship between fumarole gas composition and eruptive activity at Galeras Volcano, Colombia". *Geology* 24(6), pages 531–534. DOI: 10.1130/0091-7613(1996)024<0531:TRBFGC>2.3.CO;2.

Forte, F. M. L., A. Aiuppa, S. G. Rotolo, and V. Zanon (2023). "Temporal evolution of the Fogo Volcano magma storage system (Cape Verde Archipelago): a fluid inclusions perspective". *Journal of Volcanology and Geothermal Research* 433, page 107730. DOI: 10.1016/j.jvolgeores.2022.107730.

Gaillard, F., J. Michalski, G. Berger, S. M. McLennan, and B. Scaillet (2013). "Geochemical reservoirs and timing of sulfur cycling on Mars". *Space Science Reviews* 174(1), pages 251–300. DOI: 10.1016/j.chemgeo.2015.07.030.

Gaillard, F., B. Scaillet, and N. T. Arndt (2011). "Atmospheric oxygenation caused by a change in volcanic degassing pressure". *Nature* 478(7368), pages 229–232. DOI: 10.1038/nature10460.

Ghiorso, M. S., S. Matthews, and D. A. Sverjensky (2023). "MELTS+ DEW: Modeling major element+ Cl+ F+ S phase equilibria, redox reactions and elemental partitioning in magmatic-hydrothermal systems". In: *Goldschmidt 2023 Conference*. Goldschmidt.

Ghiorso, M. S. and G. A. R. Gualda (2015). "An H2O–CO2 mixed fluid saturation model compatible with rhyolite-MELTS". *Contributions to Mineralogy and Petrology* 169(6), page 53. DOI: 10.1007/s00410-015-1141-8.

Giggenbach, W. F. (1996). "Chemical composition of volcanic gases". In: *Monitoring and mitigation of volcano hazards*. Springer, pages 221–256. DOI: 10.1007/978-3-642-80087-0_7.

Gorojovsky, L. R. and B. J. Wood (2026). "Solubility and speciation of sulfur in silicate melts under crustal conditions". *Earth and Planetary Science Letters* 687, page 120088. DOI: 10.1016/j.epsl.2026.120088.

Helz, R. T. and C. R. Thornber (1987). "Geothermometry of Kilauea Iki lava lake, Hawaii". *Bulletin of volcanology* 49(5), pages 651–668.

Holland, T. and R. Powell (1991). "A Compensated-Redlich-Kwong (CORK) equation for volumes and fugacities of CO2 and H2O in the range 1 bar to 50 kbar and 100–1600°C". *Contributions to Mineralogy and Petrology* 109(2), pages 265–273. DOI: 10.1007/{BF}00306484.

Holloway, J. R. and J. G. Blank (1994). "Application of experimental results to COH species in natural melts". *Reviews in Mineralogy and Geochemistry* 30(1), pages 187–230. DOI: 10.1515/9781501509674-012.

Holloway, J. (1987). "Igneous fluids". *Reviews in Mineralogy and Geochemistry* 17.

Hughes, E. and L. Saper (pre-print). "Evaluation of H_2O-CO_2 solubility models in silicate melts: Precision and accuracy of vapor saturation pressure and composition". *Earth ArXiv*. DOI: 10.31223/X57J50.

Hughes, E., P. Liggins, P. Wieser, and E. Stolper (2025). "VolFe: an open-source Python package for calculating melt-vapour equilibria including silicate melt, carbon, hydrogen, sulfur, and noble gases". *Volcanica* 8(2), pages 457–481. DOI: 10.30909/vol/imvc1781.

Hughes, E. C., J. Biasi, I. Fendley, K. Rahilly, T. D. Schlieder, H. Winslow, T. P. Fischer, and P. J. Wallace (2024a). "Modeling the behavior of sulfur in magmatic systems from source to surface: Application to Whakaari/White Island, Aotearoa New Zealand, and Etna, Italy". *Journal of Volcanology and Geothermal Research* 446, page 107939. DOI: 10.1016/j.jvolgeores.2023.107939.

Hughes, E. C., P. Liggins, L. Saper, and E. M. Stolper (2024b). "The effects of oxygen fugacity and sulfur on the pressure of vapor-saturation of magma". *American Mineralogist* 109(3), pages 422–438. DOI: 10.2138/am-2022-8739.

Hughes, E. C., L. M. Saper, P. Liggins, H. S. C. O'Neill, and E. M. Stolper (2023). "The sulfur solubility minimum and maximum in silicate melt". *Journal of the Geological Society* 180(3), jgs2021–125. DOI: 10.1144/jgs2021-125.

Iacono-Marziano, G., Y. Morizet, E. L. Trong, and F. Gaillard (2012). "New experimental data and semi-empirical parameterization of H2O–CO2 solubility in mafic melts". *Geochimica et Cosmochimica Acta* 97, pages 1–23. DOI: 10.1016/j.gca.2012.08.035.

Iacovino, K., S. Matthews, P. Wieser, G. Moore, and F. Bégué (2021). "VESIcal Part I: An open-source thermodynamic model engine for mixed volatile (H2O-CO2) solubility in silicate melts". *Earth and Space Science*. DOI: 10.1029/2020ea001584.

Iacovino, K. (2015). "Linking subsurface to surface degassing at active volcanoes: a thermodynamic model with applications to Erebus volcano". *Earth and Planetary Science Letters* 431, pages 59–74. DOI: 10.1016/j.epsl.2015.09.016.

— (2021). "Ferric/Ferrous, Fe3+/FeT, fO2 Converter (Kress and Carmichael, 1991) (3.2)". *Zenodo*. DOI: https://doi.org/10.5281/zenodo.5907844.

Iacovino, K., G. Moore, K. Roggensack, C. Oppenheimer, and P. Kyle (2013). "H2O–CO2 solubility in mafic alkaline magma: applications to volatile sources and degassing behavior at Erebus volcano, Antarctica". *Contributions to Mineralogy and Petrology* 166(3), pages 845–860. DOI: 10.1007/s00410-013-0877-2.

Jugo, P. J., R. W. Luth, and J. P. Richards (2005). "Experimental data on the speciation of sulfur as a function of oxygen fugacity in basaltic melts". *Geochimica et Cosmochimica Acta* 69(2), pages 497–503. DOI: 10.1016/j.gca.2004.07.011.

Jugo, P. J., M. Wilke, and R. E. Botcharnikov (2010). "Sulfur K-edge XANES analysis of natural and synthetic basaltic glasses: Implications for S speciation and S content as function of oxygen fugacity". *Geochimica et Cosmochimica Acta* 74(20), pages 5926–5938. DOI: 10.1016/j.gca.2010.07.022.

Kern, C., A. Aiuppa, and J. M. de Moor (2022). "A golden era for volcanic gas geochemistry?" *Bulletin of Volcanology* 84(5), page 43. DOI: 10.1007/s00445-022-01556-6.

Kilburn, C. R. and A. F. Bell (2022). "Forecasting eruptions from long-quiescent volcanoes". *Bulletin of Volcanology* 84(3), page 25. DOI: 10.1007/s00445-022-01532-0.

Kress, V. C. and I. S. E. Carmichael (1991). "The compressibility of silicate liquids containing Fe2O3 and the effect of composition, temperature, oxygen fugacity and pressure on their redox states". *Contributions to Mineralogy and Petrology* 108(1-2), pages 82–92. DOI: 10.1007/bf00307328.

Le Maitre, R., A. Streckeisen, B. Zanettin, M. Le Bas, B. Bonin, and P. Bateman (2005). *Igneous Rocks: A Classification and Glossary of Terms: Recommendations of the International Union of Geological Sciences Subcommission on the Systematics of Igneous Rocks*. Cambridge University Press. ISBN: 9781139439398.

Lerner, A. H., M. J. Muth, P. J. Wallace, A. Lanzirotti, M. Newville, G. A. Gaetani, P. Chowdhury, and R. Dasgupta (2021a). "Improving the reliability of Fe-and S-XANES measurements in silicate glasses: correcting beam damage and identifying Fe-oxide nanolites in hydrous and anhydrous melt inclusions". *Chemical Geology* 586, page 120610.

Lerner, A. H., P. J. Wallace, T. Shea, A. J. Mourey, P. J. Kelly, P. A. Nadeau, T. Elias, C. Kern, L. E. Clor, C. Gansecki, et al. (2021b). "The petrologic and degassing behavior of sulfur and other magmatic volatiles from the 2018 eruption of Kilauea, Hawaii: melt concentrations, magma storage depths, and magma recycling". *Bulletin of Volcanology* 83(6), page 43.

Lesne, P., S. C. Kohn, J. Blundy, F. Witham, R. E. Botcharnikov, and H. Behrens (2011a). "Experimental Simulation of Closed-System Degassing in the System Basalt–H2O–CO2–S–Cl". *Journal of Petrology* 52(9), pages 1737–1762. DOI: 10.1093/petrology/egr027.

Lesne, P., B. Scaillet, M. Pichavant, and J.-M. Bény (2011b). "The carbon dioxide solubility in alkali basalts: an experimental study". *Contributions to Mineralogy and Petrology* 162(1), pages 153–168. DOI: 10.1007/s00410-010-0585-0.

Lev, E., S. Krasnoff, S. Charbonnier, C. Connor, A. Patra, and A. Mullins (2025). "VICTOR—A new cyberinfrastructure for volcanology". *Volcanica* 8(2), pages 563–582. DOI: 10.30909/vol/ikoj4933.

Liggins, P., S. Jordan, P. B. Rimmer, and O. Shorttle (2022). "Growth and Evolution of Secondary Volcanic Atmospheres: I. Identifying the Geological Character of Hot Rocky Planets". *Journal of Geophysical Research: Planets* 127(7). DOI: 10.1029/2021je007123.

Liggins, P., O. Shorttle, and P. B. Rimmer (2020). "Can volcanism build hydrogen-rich early atmospheres?" *Earth and Planetary Science Letters* 550, page 116546. DOI: 10.1016/j.epsl.2020.116546.

Liu, Y., Y. Zhang, and H. Behrens (2005). "Solubility of H2O in rhyolitic melts at low pressures and a new empirical model for mixed H2O–CO2 solubility in rhyolitic melts". *Journal of Volcanology and Geothermal Research* 143(1-3), pages 219–235. DOI: 10.1016/j.jvolgeores.2004.09.019.

Lloyd, A. S., T. Plank, P. Ruprecht, E. H. Hauri, and W. Rose (2013). "Volatile loss from melt inclusions in pyroclasts of differing sizes". *Contributions to Mineralogy and Petrology* 165(1), pages 129–153. DOI: 10.1007/s00410-012-0800-2.

Lowenstern, J. B., J. Thompson, et al. (1995). "Applications of silicate-melt inclusions to the study of magmatic volatiles". *Magmas, fluids and ore deposits* 23, pages 71–99.

Metrich, N. and P. J. Wallace (2008). "Volatile abundances in basaltic magmas and their degassing paths tracked by melt inclusions". *Reviews in mineralogy and geochemistry* 69(1), pages 363–402. DOI: 10.2138/rmg.2008.69.10.

Mickus, K. (2003). "Gravity Constraints on the Crustal Structure of Central America". In: *The Circum-Gulf of Mexico and the Caribbean: Hydrocarbon habitats, basin formation, and plant tectonics.* Edited by C. Bartonlini, R. T. Buffler, and J. Blickwede. Volume 79. AAPG Memoir. AAPG. Chapter 29, pages 638–655.

Moore, G. M., T. Vennemann, and I. Carmichael (1998). "An empirical model for the solubility of H2O in magmas to 3 kilobars". *American Mineralogist* 83, pages 36–42.

Moore, L. R., E. Gazel, R. Tuohy, A. S. Lloyd, R. Esposito, M. Steele-MacInnis, E. H. Hauri, P. J. Wallace, T. Plank, and R. J. Bodnar (2015). "Bubbles matter: An assessment of the contribution of vapor bubbles to melt inclusion volatile budgets". *American Mineralogist* 100(4), pages 806–823.

Moretti, R., P. Papale, and G. Ottonello (2003). "Volcanic Degassing". In: Geological Society of London. Chapter A model for the saturation of COHS fluids in silicate melts. DOI: 10.1144/GSL.SP.2003.213.01.06.

Moretti, R. and P. Papale (2004). "On the oxidation state and volatile behavior in multicomponent gas–melt equilibria". *Chemical Geology* 213(1-3), pages 265–280. DOI: 10.1016/j.chemgeo.2004.08.048.

Moussallam, Y., M. Edmonds, B. Scaillet, N. Peters, E. Gennaro, I. Sides, and C. Oppenheimer (2016). "The impact of degassing on the oxidation state of basaltic magmas: a case study of Kılauea volcano". *Earth and Planetary Science Letters* 450, pages 317–325.

Muth, M. J. and P. J. Wallace (2021). "Slab-derived sulfate generates oxidized basaltic magmas in the southern Cascade arc (California, USA)". *Geology*. DOI: 10.1130/g48759.1.

Nash, W. M., D. J. Smythe, and B. J. Wood (2019). "Compositional and temperature effects on sulfur speciation and solubility in silicate melts". *Earth and Planetary Science Letters* 507. DOI: 10.1016/j.epsl.2018.12.006.

Newcombe, M., A. Brett, J. Beckett, M. Baker, S. Newman, Y. Guan, J. Eiler, and E. Stolper (2017). "Solubility of water in lunar basalt at low pH2O". *Geochimica et Cosmochimica Acta* 200, pages 330–352. DOI: 10.1016/j.gca.2016.12.026.

Newcombe, M. E., T. Plank, Y. Zhang, M. Holycross, A. Barth, A. S. Lloyd, D. Ferguson, B. F. Houghton, and E. Hauri (2020). "Magma Pressure-Temperature-Time Paths During Mafic Explosive Eruptions". *Frontiers in Earth Science* 8, page 531911. DOI: 10.3389/feart.2020.531911.

Newman, S. and J. B. Lowenstern (2002). "VolatileCalc: a silicate melt–H2O–CO2 solution model written in Visual Basic for excel". *Computers & Geosciences* 28(5), pages 597–604. DOI: 10.1016/s0098-3004(01)00081-4.

Nzotta, M. M., D. Sichen, and S. Seetharaman (1999). "A study of the sulfide capacities of iron-oxide containing slags". *Metallurgical and Materials Transactions B* 30(5), pages 909–920. DOI: 10.1007/s11663-999-0096-4.

O'Neill, H. S. (2021). "Magma Redox Geochemistry". *Geophysical Monograph Series*, pages 177–213. DOI: 10.1002/9781119473206.ch10.

O'Neill, H. S. and J. A. Mavrogenes (2022). "The sulfate capacities of silicate melts". *Geochimica et Cosmochimica Acta* 334, pages 368–382. DOI: 10.1016/j.gca.2022.06.020.

O'Neill, H. S. C. and J. A. Mavrogenes (2002). "The sulfide capacity and the sulfur content at sulfide saturation of silicate melts at 1400 C and 1 bar". *Journal of Petrology* 43(6), pages 1049–1087.

Ohmoto, H. and D. M. Kerrick (1977). "Devolatilization equilibria in graphitic systems". *American Journal of Science* 277(8), pages 1013–1044. DOI: 10.2475/ajs.277.8.1013.

Oppenheimer, C. (2010). "Ultraviolet sensing of volcanic sulfur emissions". *Elements* 6(2), pages 87–92. DOI: 10.2113/gselements.6.2.87.

Oppenheimer, C., R. Moretti, P. R. Kyle, A. Eschenbacher, J. B. Lowenstern, R. L. Hervig, and N. W. Dunbar (2011). "Mantle to surface degassing of alkalic magmas at Erebus volcano, Antarctica". *Earth and Planetary Science Letters* 306(3-4), pages 261–271. DOI: 10.1016/j.epsl.2011.04.005.

Papale, P., R. Moretti, and A. Paonita (2022). "Thermodynamics of multi-component gas–melt equilibrium in magmas: theory, models, and applications". *Reviews in Mineralogy and Geochemistry* 87(1), pages 431–556. DOI: 10.2138/rmg.2022.87.10.

Peng, D.-Y. and D. B. Robinson (1976). "A New Two-Constant Equation of State". *Industrial & Engineering Chemistry Fundamentals* 15(1), pages 59–64. DOI: 10.1021/i160057a011.

Poland, M. P. and K. R. Anderson (2020). "Partly cloudy with a chance of lava flows: Forecasting volcanic eruptions in the twenty-first century". *Journal of Geophysical Research: Solid Earth* 125(1), e2018JB016974. DOI: 10.1029/2018JB016974.

Rasmussen, D. J., T. A. Plank, P. J. Wallace, M. E. Newcombe, and J. B. Lowenstern (2020). "Vapor-bubble growth in olivine-hosted melt inclusions". *American Mineralogist* 105(12), pages 1898–1919.

Roedder, E. (1979). "Origin and significance of magmatic inclusions". *Bulletin de Mineralogie* 102(5), pages 487–510.

Rose-Koga, E. F., A.-S. Bouvier, G. Gaetani, P. Wallace, C. Allison, J. Andrys, C. A. De La Torre, A. Barth, R. Bodnar, A. B. Gartner, et al. (2021). "Silicate melt inclusions in the new millennium: A review of recommended practices for preparation, analysis, and data presentation". *Chemical Geology* 570, page 120145. DOI: 10.1016/j.chemgeo.2021.120145.

Scaillet, B. and M. Pichavant (2004). "Role of fO_2 on fluid saturation in oceanic basalt". *Nature* 430. DOI: 10.1038/nature02814.

Shi, P. and S. K. Saxena (1992). "Thermodynamic modeling of the C-H-O-S fluid system". *American Mineralogist* 77, pages 1038–1049.

Shinohara, H., K. Kazahaya, G. Saito, K. Fukui, and M. Odai (2003). "Variation of CO2/SO2 ratio in volcanic plumes of Miyakejima: Stable degassing deduced from heliborne measurements". *Geophysical Research Letters* 30(5). DOI: 10.1029/2002GL016105.

Shishkina, T. A., R. E. Botcharnikov, F. Holtz, R. R. Almeev, A. M. Jazwa, and A. A. Jakubiak (2014). "Compositional and pressure effects on the solubility of H2O and CO2 in mafic melts". *Chemical Geology* 388, pages 112–129. DOI: 10.1016/j.chemgeo.2014.09.001.

Sides, I., M. Edmonds, J. Maclennan, B. F. Houghton, D. Swanson, and M. J. Steele-MacInnis (2014). "Magma mixing and high fountaining during the 1959 Kılauea Iki eruption, Hawai 'i". *Earth and Planetary Science Letters* 400, pages 102–112.

Simon, A. C. and M. Wilke (2026). "The Behavior of Sulfur in Silicate Melts". In: *The Role of Sulfur in Planetary Processes: From Cores to Atmospheres*. Cham: Springer Nature Switzerland, pages 859–940. ISBN: 978-3-032-07705-9. DOI: 10.1007/978-3-032-07705-9_12.

Stix, J. and J. de Moor (2018). "Understanding and forecasting phreatic eruptions driven by magmatic degassing". *Earth Planets Space* 70(83). DOI: 10.1186/s40623-018-0855-z.

Sun, C. and C.-T. A. Lee (2022). "Redox evolution of crystallizing magmas with C-H-O-S volatiles and its implications for atmospheric oxygenation". *Geochimica et Cosmochimica Acta* 338, pages 302–321. DOI: https://doi.org/10.1016/j.gca.2022.09.044.

Sun, C. and L. Yao (2024). "Redox equilibria of iron in low- to high-silica melts: A simple model and its applications to C-H-O-S degassing". *Earth and Planetary Science Letters* 638, page 118742. DOI: https://doi.org/10.1016/j.epsl.2024.118742.

— (2026). "A unified H2O–CO2 solubility–speciation model for magmatic liquids: Constraints on magma storage architecture in continental rifts". *Earth and Planetary Science Letters* 689, page 120115. DOI: 10.1016/j.epsl.2026.120115.

Sutton, A. J. and T. Elias (2014). "One Hundred Volatile Years of Volcanic Gas Studies at the Hawaiian Volcano Observatory". In: *Characteristics of Hawaiian Volcanoes*. Edited by M. P. Poland, T. J. Takahashi, and C. M. Landowski. Volume 1801. U.S. Geological Survey Professional Paper, pages 295–320. ISBN: 2330-7102. DOI: 10.3133/pp18017.

Taracsák, Z., T. Mather, S. Ding, T. Plank, M. Brounce, D. Pyle, A. Aiuppa, et al. (2023). "Sulfur from the subducted slab dominates the sulfur budget of the mantle wedge under volcanic arcs". *Earth and Planetary Science Letters* 602, page 117948. DOI: 10.1016/j.epsl.2022.117948.

Theunissen, T., R. S. Huismans, G. Lu, and N. Riel (2022). "Relative continent - mid-ocean ridge elevation: A reference case for isostasy in geodynamics". *Earth-Science Reviews* 233, page 104153. DOI: 10.1016/j.earscirev.2022.104153.

Thibault, Y. and J. R. Holloway (1994). "Solubility of CO2 in a Ca-rich leucitite: effects of pressure, temperature, and oxygen fugacity". *Contributions to Mineralogy and Petrology* 116(1-2), pages 216–224. DOI: 10.1007/bf00310701.

Thomas, R. W. and B. J. Wood (2026). "Sulfur speciation in silicate melts at high pressure". *Geochimica et Cosmochimica Acta* 417, pages 37–51. DOI: 10.1016/j.gca.2026.02.003.

Tucker, J. M., E. H. Hauri, A. J. Pietruszka, M. O. Garcia, J. P. Marske, and F. A. Trusdell (2019). "A high carbon content of the Hawaiian mantle from olivine-hosted melt inclusions". *Geochimica et Cosmochimica Acta* 254, pages 156–172.

Wallace, P. J. and I. S. Carmichael (1994). "S speciation in submarine basaltic glasses as determined by measurements of S Kα X-ray wavelength shifts". *American Mineralogist* 79(1-2), pages 161–167.

Wardell, L. J., P. R. Kyle, N. Dunbar, and B. Christenson (2001). "White Island volcano, New Zealand: carbon dioxide and sulfur dioxide emission rates and melt inclusion studies". *Chemical Geology* 177(1-2), pages 187–200. DOI: 10.1016/S0009-2541(00)00391-0.

Webster, J. D. and R. E. Botcharnikov (2011). "Distribution of sulfur between melt and fluid in SOHC-Cl-bearing magmatic systems at shallow crustal pressures and temperatures". *Reviews in Mineralogy and Geochemistry* 73(1), pages 247–283. DOI: 10.2138/rmg.2011.73.9.

Werner, C., P. J. Kelly, M. Doukas, T. Lopez, M. Pfeffer, R. McGimsey, and C. Neal (2013). "Degassing of CO2, SO2, and H2S associated with the 2009 eruption of Redoubt Volcano, Alaska". *Journal of Volcanology and Geothermal Research* 259, pages 270–284. DOI: 10.1016/j.jvolgeores.2012.04.012.

Werner, C., D. J. Rasmussen, T. Plank, P. J. Kelly, C. Kern, T. Lopez, J. Gliss, J. Power, D. Roman, P. Izbekov, et al. (2020). "Linking subsurface to surface using gas emission and melt inclusion data at Mount Cleveland volcano, Alaska". *Geochemistry, Geophysics, Geosystems* 21(7), e2019GC008882. DOI: 10.1029/2019GC008882DigitalObjectIdentifier(DOI).

Werner, C. A., M. P. Doukas, and P. J. Kelly (2011). "Gas emissions from failed and actual eruptions from Cook Inlet Volcanoes, Alaska, 1989–2006". *Bulletin of Volcanology* 73(2), pages 155–173. DOI: 10.1007/s00445-011-0453-4.

Wieser, P. E., K. Iacovino, S. Matthews, G. Moore, and C. M. Allison (2022). "VESIcal Part II: A critical approach to volatile solubility modelling using an open-source Python3 engine". *Earth and Space Science*. DOI: 10.1029/2021ea001932.

Wieser, P. and M. Gleeson (2023). "PySulfSat: An open-source Python3 tool for modeling sulfide and sulfate saturation". *Volcanica* 6(1), pages 107–127.

Wieser, P. E., F. Jenner, M. Edmonds, J. Maclennan, and B. E. Kunz (2020). "Chalcophile elements track the fate of sulfur at Kılauea Volcano, Hawai'i". *Geochimica et Cosmochimica Acta* 282, pages 245–275.

Wieser, P. E., H. Lamadrid, J. Maclennan, M. Edmonds, S. Matthews, K. Iacovino, F. E. Jenner, C. Gansecki, F. Trusdell, R. L. Lee, et al. (2021). "Reconstructing magma storage depths for the 2018 Kilauean eruption from melt inclusion CO2 contents: the importance of vapor bubbles". *Geochemistry, Geophysics, Geosystems* 22(2), e2020GC009364.

Wieser, P. E., S. C. Shi, M. L. Gleeson, B. Rangel, C. L. DeVitre, A. T. Bearden, K. J. Lynn, and M. Camille-Caumon (2025). "Fluid inclusion constraints on the geometry of the magmatic plumbing system beneath Mauna Loa—part 1: Lavas and tephras". *Bulletin of Volcanology* 87(10), page 89. DOI: 10.1007/s00445-025-01874-5.

Wilkinson, M. D., M. Dumontier, J. Aalbersberg, G. Appleton, M. Axton, A. Baak, N. Blomberg, J.-W. Boiten, L. B. d. S. Santos, P. E. Bourne, J. Bouwman, A. J. Brookes, T. Clark, M. Crosas, I. Dillo, O. Dumon, S. Edmunds, C. T. Evelo, R. Finkers, A. Gonzalez-Beltran, A. J. Gray, P. Groth, C. Goble, J. S. Grethe, J. Heringa, P. A. Hoen, R. Hooft, T. Kuhn, R. Kok, J. Kok, S. J. Lusher, M. E. Martone, A. Mons, A. L. Packer, B. Persson, P. Rocca-Serra, M. Roos, R. v. Schaik, S.-A. Sansone, E. Schultes, T. Sengstag, T. Slater, G. Strawn, M. A. Swertz, M. Thompson, J. v. d. Lei, E. v. Mulligen, J. Velterop, A. Waagmeester, P. Wittenburg, K. Wolstencroft, J. Zhao, and B. Mons (2016). "The FAIR Guiding Principles for scientific data management and stewardship". *Scientific Data* 3(1), page 160018. DOI: 10.1038/sdata.2016.18.

Witham, F., J. Blundy, S. C. Kohn, P. Lesne, J. Dixon, S. V. Churakov, and R. Botcharnikov (2012). "SolEx: A model for mixed COHSCl-volatile solubilities and exsolved gas compositions in basalt". *Computers & Geosciences* 45(Chemical Geology 263 2009), pages 87–97. DOI: 10.1016/j.cageo.2011.09.021.

Yoshimura, S. (2023). "Carbon dioxide and water in the crust. Part 1: Equation of state for the fluid". *Journal of Mineralogical and Petrological Sciences* 118(1), 221224a.